

Magnus Staur

Support Design for Mine Drifts

Principals, Methodologies and Implementation

Specialisation project in Geosciences
Supervisor: Hakan Basarir
December 2024

Norwegian University of Science and Technology
Faculty of Engineering
Department of Geoscience



Abstract

This report presents a comprehensive overview of support design principles, methodologies, and implementation for underground mining operations, focusing on hard rock conditions. The study incorporates fundamental concepts of rock mechanics, such as intact rock properties, joint systems, stress conditions, and failure criteria, which are critical for understanding support design.

Empirical methods, which rely on classification systems like RMR and Q-values, provide a practical starting point but are limited by idealized assumptions. Analytical methods, such as the Convergence-Confinement Method (CCM), enhance understanding of rock-support interaction but may oversimplify real-world complexities. Numerical modeling, including techniques like FEM, offers the most advanced insights by simulating stress distribution, deformation, and failure mechanisms under varying conditions.

Combining these methods provides a robust and systematic framework for support design that accounts for site-specific geological and stress environments, ensuring stability and safety in underground excavations.

Preface

This report is submitted as part of the course TGB4580 - Mineral Production and Technical Resource Geology, a specialization project in the fifth year of the Technical Geosciences program at NTNU Trondheim. The purpose of the course is to teach students scientific working methods by completing an independent project within their field of study. The project is also intended to provide a strong scientific foundation for the master's thesis, which will be written in the following semester.

The report focuses on support design in underground mining and presents methods that will be used in my master's thesis. The thesis will utilise data from Rana Gruber, an iron ore mine in Mo i Rana, to develop a support design based on these methods.

This report can also serve as a fundamental introduction to the basic methods used in rock mass engineering for future students, while referencing scientific reports to further expand their understanding of the topics.

Contents

Abstract	i
Preface	ii
Contents	v
List of Figures	v
List of Tables	vii
Abbreviations	ix
1 Introduction	1
1.1 Background and Importance of Drift Support Design	1
1.2 Objectives of the Study	2
1.3 Scope and Limitations	2
2 Fundamental Concepts in Drift Support Design	4
2.1 Rock Properties	5

2.1.1	Intact Rock Properties	5
2.1.2	Joint Properties	12
2.1.3	Rock Mass Design Parameters	16
2.2	Stress Conditions	19
2.3	Geometry	25
2.4	Rock Stabilisation Measures	28
2.4.1	Rock Reinforcement	28
2.4.2	Rock Support	31
2.5	Failure Criteria	32
2.5.1	Mohr-Coulomb Failure Criterion	32
2.5.2	Hoek-Brown Failure Criterion	37
3	Support Design Methodologies	45
3.1	Empirical Design Methods	46
3.1.1	Rock Quality Designation	47
3.1.2	Rock Mass Rating	49
3.1.3	Q-system	52
3.1.4	Geological Strength Index	58
3.1.5	Calculation of Rock Mass Design Parameters Using Rock Mass Classification and Characterization Systems	63
3.1.6	Comparison of Empirical Methods	67
3.1.7	Applications and Limitations	70
3.2	Analytical Design Methods	70
3.2.1	Convergence-Confinement Method	70

3.2.2	Applications and Limitations	73
3.3	Numerical Modelling Approaches	74
3.3.1	Continuum Methods	75
3.3.2	Discontinuum Methods	78
3.3.3	Applications and Limitations	80
4	Conclusions	83
	References	83
	Appendices	89
A	RQD	90
B	RMR₈₉ and RMR₁₄ Tables	95

List of Figures

2.1.1 Overview of intact rock and discontinuities making up the rockmass	6
2.1.2 Cut-away view of Hoek triaxial cell	8
2.1.3 JRC	13
2.1.4 Direct shear test on a rock joint	15
2.1.5 The influence of scale on jointed rock masses	18
2.2.1 An overview of the stress terminology	20
2.2.2 Vertical stress measurement around the world	22
2.2.3 Relationship between depth and the ratio of horizontal to vertical stress k	23
2.2.4 Illustration of stress redistribution around an excavation	24
2.3.1 Stress concentrations around an excavation in a uniform stress field	26
2.5.1 Non-linear failure envelope derived from multiple Mohr's circles	34
2.5.2 MC failure criterion in τ - σ and σ_1 - σ_3 systems	36
2.5.3 Linear MC criterion using Mohr's circle	36
2.5.4 Adjusting the Hoek–Brown failure envelope	40

2.5.5 Choice of failure criterion	41
2.5.6 Flowchart for using the Generalised Hoek-Brown criterion	42
3.1.1 Stand-up time as a function of unsupported span	51
3.1.2 Rock Support Chart for the Q-system	56
3.1.3 Basic chart for GSI	60
3.1.4 Quantification of GSI by Joint Condition and RQD	62
3.2.1 Circular opening under hydrostatic stress field	71
3.2.2 Interaction between LDP, GRC, and SRC	72
3.3.1 Horseshoe-shaped drift with varying support levels	79
3.3.2 Rock mass conditions and numerical methods	81
A.0.1RQD Example	91
A.0.2RQD Sydney test	94
B.0.1RMR ₈₉ input parameters	98
B.0.2Support recommendations by RMR ₈₉	99

List of Tables

2.1.1 Presentation of Rock Mass Design Parameters	17
2.5.1 Field estimates of uniaxial compressive strength	43
2.5.2 Estimated values for m_i by rock group	44
3.1.1 Rock Quality Designation (RQD) classification and corresponding quality ranges.	48
3.1.2 Empirical equations for calculating E_m	64
3.1.3 Empirical equations for calculating σ_{cm}	65
3.1.4 Empirical equations for calculating σ_{tm}	65
3.1.5 Empirical equations for calculating ν_m	66
3.1.6 Empirical equations for calculating c_m and ϕ_m	66
A.0.1 RQD Rock Mass Classification	90

Abbreviations

List of all abbreviations in alphabetic order:

- **BEM** Boundary Element Method
- **CCM** Convergence-Confinement Method
- **DEM** Discrete Element Method
- **DFN** Discrete Fracture Network Method
- **ED-FEM** Embedded Discontinuity-FEM
- **ESR** Excavation Support Ratio
- **FDM** Finite Difference Method
- **FEM** Finite Element Method
- **G-FEM** Generalised-FEM
- **GRC** Ground Reaction Curve
- **GSI** Geological Strength Index
- **HB** Hoek-Brown Failure Criterion
- **IGV** Faculty for Geosciences
- **JCond₈₉** Condition of Discontinuities
- **LDP** Longitudinal Displacement Profile
- **MC** Mohr-Coulomb Failure Criterion

- **NTNU** Norwegian University of Science and Technology
- **Q** Q-system
- **RMR** Rock Mass Rating
- **RQD** Rock Quality Designation
- **RRS** Fiber Reinforced Ribs of Sprayed Concrete
- **RS2** Rock and Soil 2-Dimensional Analysis Program
- **SRC** Support Reaction Curve
- **SFRS** Steel Fiber-Reinforced Shotcrete
- **UCS** Uniaxial Compressive Strength
- **X-FEM** Extended-FEM

Chapter 1

Introduction

1.1 Background and Importance of Drift Support Design

An optimised support design is essential for the safety, efficiency, and profitability of underground mining operations. Its primary purpose is to prevent collapse, rockfall, rockburst, and other stability-related issues, ensuring a safe working environment while controlling costs (E. Hoek, P. K. Kaiser, et al., 2000).

Inadequate support design poses significant risks to both worker safety and equipment integrity. Rockfalls, for instance, can dilute ore by causing failure in the rock surrounding a stope, while instabilities can delay operations if not promptly addressed (E. Hoek, P. K. Kaiser, et al., 2000). Such challenges can reduce profitability and jeopardise the overall sustainability of mining operations.

Stability issues in underground mining are observed at two distinct scales. The first is the mine scale, which encompasses the entire mining operation, including the ore body, infrastructure, and surrounding rock mass. Mine-scale stability challenges depend on factors such as the ore body's natural characteristics and geometry, surrounding rock mass properties, stress conditions, excavation methods, and sequencing (E. Hoek, P. K. Kaiser, et al., 2000).

The second scale is more localised, focusing on specific areas such as a footwall drift or a single stope. Local stability is influenced by the stress state and structural conditions within a few tens of meters from the excavation boundary (E. Hoek, P. K. Kaiser, et al., 2000).

The advancement of support systems, combined with an improved understanding of rock mechanics, has enabled mining operations to extend deeper into the earth's crust in search of valuable minerals. However, as mining depth increases, so does the importance of effective support design. The deeper environment is characterised by higher stresses, particularly dynamic stress conditions, making support design more challenging and critical (E. Hoek, P. K. Kaiser, et al., 2000).

1.2 Objectives of the Study

Relying solely on subjective judgment for support design, can lead to both over- and under-dimensioned solutions that are not suited to the conditions. Therefore, engineers should have a solid understanding of the fundamental concepts that influence support design and apply well-established methods in the design process (Evert Hoek, 2007).

The primary objective of this study is to develop a fundamental understanding of the three main approaches to support design: empirical, analytical, and numerical methods that can be applied on a local scale in a mine drift.

1.3 Scope and Limitations

This study focuses on support design for hard rock mining, excluding considerations for soft rock masses. It covers fundamental concepts in rock engineering, including intact rock properties, rock mass properties, stress conditions, excavation geometry, rock stabilisation measures, and failure criteria.

The empirical methods section explores rock mass classification systems such as RMR and Q, as well as the GSI characterization system. Analytical methods cover key components such as the Ground Reaction Curve (GRC), Support Reaction Curve (SRC), and Longitudinal Deformation Profile (LDP).

Numerical methods introduce modelling techniques, including the finite element method (FEM), RS2 software, and approaches for input data calibration and model validation.

Applications and limitations of each method are discussed, emphasizing their practical application in support design.

Chapter 2

Fundamental Concepts in Drift Support Design

Drift support design refers to the process of planning and implementing support measures to stabilise underground excavations in rock. The goal of drift support design is to ensure that the rock mass surrounding the excavation remains stable throughout its lifecycle. Support design must address how the rock mass behaves both during and after excavation and involves selecting and placing support elements based on the unique characteristics and stability requirements of the site (Evert Hoek and P. Kaiser, 1995).

Excavating in rock is a complex task influenced by numerous critical factors. In applied rock mechanics, three primary factors are crucial: the quality of the rock mass, in situ stresses, and the geometry of the excavation. The quality of the rock mass is defined by the mechanical properties of the (intact) rock material, water conditions, and the characteristics of any discontinuities. How the rock mass responds to excavation also depends on the existing stress conditions, as well as the shape and size of the opening (Evert Hoek and P. Kaiser, 1995).

While in situ stresses and rock quality are defined by natural geological conditions and cannot be modified, the geometry of the excavation can be adjusted. Here, engineering design plays a pivotal role, using knowledge of the rock mass and stress environment to optimise excavation geometry and create an effective support system tailored to the excavation's intended use. By adjusting the shape, size, and orientation of the opening, engineers can min-

imise stress concentrations and enhance the overall stability of the structure (Evert Hoek and P. Kaiser, 1995).

This chapter will cover the fundamental concepts essential for drift support design, starting with the properties of intact rock and joint properties, which determine the inherent strength and behaviour of the rock mass. Following this, stress conditions, including both *in situ* and induced stresses, will be presented to provide insight into how stresses influence excavation stability and support needs. The chapter will then address the importance of excavation geometry and various stabilisation elements that can be used to stabilise rock around an opening. Finally, failure criteria, such as the Mohr-Coulomb and Hoek-Brown, will be explored to understand the limits of rock strength. Together, these topics establish the foundation needed to design effective support systems.

2.1 Rock Properties

To understand the behaviour of rock mass, it is necessary to study the intact rock material as well as the discontinuities that make up the rock mass (Evert Hoek, 2007). Figure 2.1.1 illustrates the fundamental components that must be accounted for.

2.1.1 Intact Rock Properties

Intact rock (or rock material) properties refer to the natural properties of the rock itself, excluding structural features such as discontinuities. The most important mechanical properties of intact rock are strength and elasticity (C. Li, 2021).

Intact rock primarily possesses two types of strength: compressive and tensile. These strengths can be determined through various laboratory tests, including the uniaxial compressive strength test, triaxial compressive strength test, direct tensile test, point load test, and brazilian test. The elasticity properties, such as the deformation modulus E_i and Poisson's ratio ν_i , can also be derived from some of these tests (C. Li, 2021). This subsection introduces the most important tests and concepts related to the strength and elasticity of intact rock.

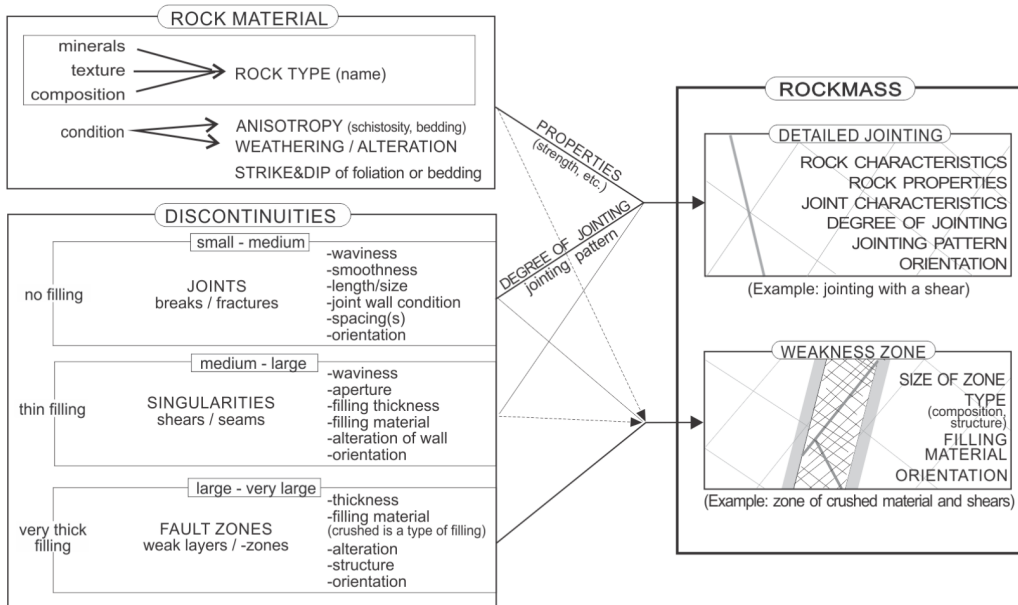


Figure 2.1.1: Overview of intact rock and discontinuities making up the rockmass (*RockMass* 2024).

2.1.1.1 Intact Rock Strength

The failure of intact rock plays a significant role in determining the overall failure of rock masses (Evert Hoek, 2007). Accurately determining the strength of intact rock is therefore essential for support design.

Compressive strength is a critical parameter for designing underground excavations. It represents the maximum axial stress a rock can endure before failure under compression. Tests such as the uniaxial compressive strength (UCS) test, the triaxial compression test, and the point load index test are commonly used to determine this property.

The UCS is typically lower for sedimentary rocks and higher for igneous rocks. Average values for shales and chist are 33-43 MPa and above 300 MPa for diabase and dolerite (Evert Hoek, 2007). The large range highlights the importance of understanding strength at a given site.

Tensile strength is the maximum stress a rock can withstand in tension before failure. Rocks are generally much weaker in tension than in compression, and is important for understanding potential cracking. To evaluate tensile strength, the direct tensile strength test and the Brazilian test (indirect ten-

sile strength test) are typically performed (Evert Hoek, 2007).

Uniaxial Compressive Strength Test

A uniaxial compressive strength (UCS) test is commonly performed to determine the mechanical properties of rock samples. It measures the compressive strength of a rock without any confining pressure. A cylindrical rock specimen with predetermined dimensions is subjected to an axial load (P), and the applied stress (σ) is calculated as the load divided by the cross-sectional area of the core. The UCS is defined as:

$$UCS = \sigma_c = \frac{P_{max}}{A} \quad (2.1)$$

where A is the cross-sectional area of the specimen (C. Li, 2021).

During the test, both axial and lateral strain are measured using strain gauges or Linear Variable Displacement Transducers (LVDTs) attached to the specimen. The results are plotted as stress (σ_1) versus strain (ϵ), revealing the rock's behaviour under load. To ensure reliability, at least five approved tests should be conducted. The gathered data can be used to calculate key parameters such as the deformation modulus (E_i), Poisson's ratio (ν_i), cohesion (c_i), friction angle (ϕ_i), and the UCS itself (C. Li, 2021).

Triaxial Compression Test

The triaxial compression test builds on the UCS test by introducing confining stress (σ_2 and σ_3) to simulate in-situ stress conditions. In conventional triaxial testing, the confining stress is equal in all lateral directions ($\sigma_2 = \sigma_3$). The specimen is placed inside a pressure cell with an oil medium providing the confining stress. The rock is isolated in a protective jacket to prevent oil intrusion (C. Li, 2021). A triaxial cell can be seen in Figure 2.1.2.

As the axial load increases, both axial and lateral strains are measured and plotted. Higher confining pressure leads to increased peak strength. The peak strength can increase by a factor of three to five under confining pressure. Residual strength also rises, approaching the peak strength as confining stress increases (Evert Hoek, 2007).

There is a behaviour change of the intact rock at higher confining stress. At low confining stress, the behaviour is usually brittle, and failure happens suddenly and catastrophically, with little deformation occurring before failure.

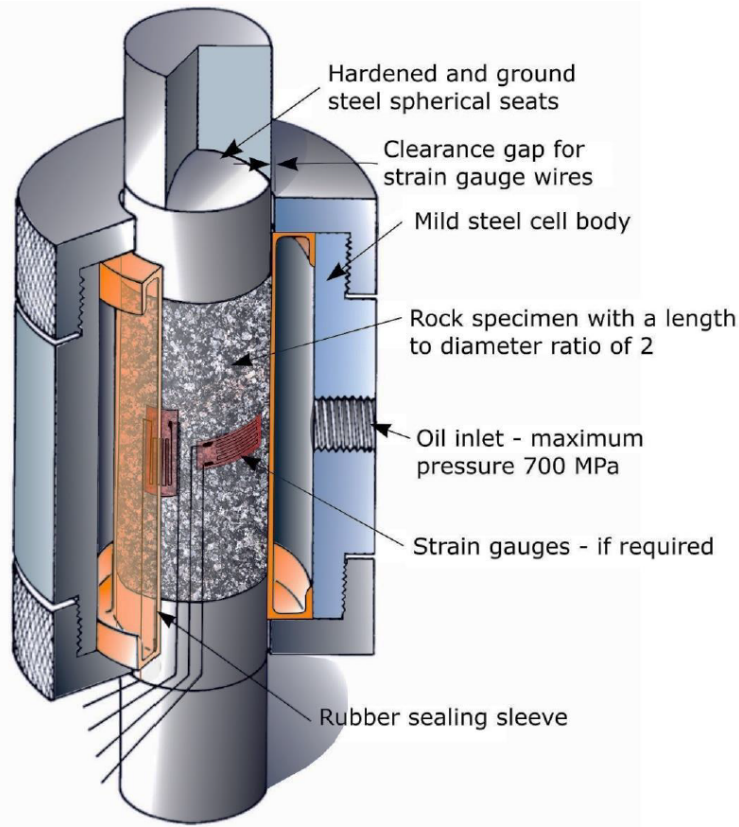


Figure 2.1.2: Cut-away view of Hoek triaxial cell (Evert Hoek, 2007).

At higher confining stress, the behaviour becomes ductile, and the rock deforms plastically (permanently) without sudden failure. The brittle-ductile transition usually occurs in the range $3 < \sigma_1/\sigma_3 < 5$ (Evert Hoek, 2007).

With triaxial tests on rock samples, one can obtain the same data as in a UCS test, but with the added benefit of testing under varying stress conditions. Residual data, which is essential for applications such as plastic analysis, can also be collected in both UCS and triaxial tests. This includes parameters such as residual cohesion (c_{res}), residual friction angle (ϕ_{res}), residual dilation (ψ_{res}), residual deformation modulus (E_{res}) and the dilation angle (i) (C. Li, 2021).

To achieve reliable results, a triaxial testing program should include at least five tests, preferably at different confining pressures that reflect the site conditions (Evert Hoek, 2007).

Point Load Test

The point load test is a faster and more economical alternative to the uniaxial compressive strength test and is widely accepted globally. Its portability allows testing to be performed on-site using either core samples or irregular rock specimens. While individual results may vary significantly, the ability to conduct multiple tests quickly ensures that the average value provides a reliable estimate of the rock's UCS (C. Li, 2021).

In this test, a rock specimen is placed between two platens, and a force P is manually applied until failure occurs. The point load index, I_s is calculated as (C. Li, 2021):

$$I_s = \frac{P}{D_e^2} \quad (2.2)$$

Here, D_e is the *equivalent core diameter*, a standardised parameter to ensure comparability between test results for specimens of different sizes and shapes:

- For core specimens with a diameter of 50 mm, $D_e = D$, where D is the core diameter.
- For irregular lump specimens, D_e is calculated as:

$$D_e = \sqrt{\frac{4A}{\pi}}$$

where A is the minimum cross-sectional area of the specimen, determined as $A = W \cdot D$. Here, W is the average width of the minimum cross section, and D is the distance between the loading points (C. Li, 2021).

To standardise the point load index to a core diameter of 50 mm, a size correction factor, F , is applied (C. Li, 2021):

$$I_{s(50)} = F \cdot I_s \quad (2.3)$$

The correction factor F is given by (C. Li, 2021):

$$F = \left(\frac{D_e}{50} \right)^{0.45} \quad (2.4)$$

Finally, the UCS is estimated using the standardised point load index, $I_{s(50)}$, through the following empirical relationship (C. Li, 2021):

$$\sigma_c = 22 \cdot I_{s(50)} \quad (2.5)$$

This relationship provides an approximate UCS value based on the point load test, making it a practical and efficient method for preliminary rock strength evaluation (C. Li, 2021).

Direct Tensile Test

The direct tensile test is the most accurate method for determining the true tensile strength of rock, but it is challenging to obtain reliable results due to difficulties in specimen preparation (Evert Hoek, 2007). The test involves gluing steel platens to either end of a core sample and applying a pulling force P across an area A . The tensile strength (σ_t) is calculated as (C. Li, 2021):

$$\sigma_t = \frac{P}{A} \quad (2.6)$$

Brazilian Test

Due to the challenges associated with direct tensile testing, the Brazilian test is a widely used alternative for evaluating tensile strength. This indirect tensile strength test applies load in the diametral direction, inducing tensile stresses in the middle of the sample along the line connecting the loading points (C. Li, 2021).

A core sample is placed between two jaws, which press against the specimen as a load P is manually applied. The recommended diameter D of the core is 50 mm, and the thickness t should equal $0.5 \cdot D$. The failure must occur along the diametral line, and multiple tests are recommended to calculate an average tensile strength. The tensile strength is determined using the formula (C. Li, 2021):

$$\sigma_t = \frac{2}{\pi} \cdot \frac{P}{D \cdot t} \quad (2.7)$$

2.1.1.2 Intact Rock Elasticity and Deformation

Elasticity is the ability of a rock material to deform under stress and return to its original shape once the stress is removed, provided the deformation remains within the elastic range. This behaviour is described by Hooke's Law, the fundamental principle of elasticity theory. Hooke's Law states that strain in a material is directly proportional to the applied stress, as long as the material stays within its elastic limit. Two important parameters related to elastic deformation of rock are the elastic modulus (deformation modulus, E) and Poisson's ratio (ν) (C. Li, 2021).

The stress-strain relationship of a rock material in a UCS or triaxial test is generally not linear. However, an early section of the stress-strain curve is linearly elastic. Both E_i and ν_i are calculated using data from this section of the stress-strain curve (C. Li, 2021).

The deformation modulus measures the stiffness of the rock material, describing how much it deforms under axial stress. It is calculated as the ratio of axial stress (σ_a) to axial strain (ϵ_a) within the elastic range of the material. This is typically calculated at approximately 50% of the maximum axial stress (C. Li, 2021):

$$E_i = \frac{\Delta \sigma_{a,50\%}}{\Delta \epsilon_{a,50\%}} \quad (2.8)$$

Higher values of E_i indicate stiffer materials that deform less under stress, while lower values represent more flexible or less stiff rocks. Typical values for E_i range from 8 to 127 GPa, with rocks such as shales, schists, and claystones falling on the lower end of the spectrum, and quartzite, gabbro, and dolerite on the higher end. In general, sedimentary rocks tend to have lower E_i values, while igneous rocks exhibit higher values. Metamorphic rocks show a broader range of E_i values. Both the strength and the deformation modulus of rock decrease with increasing water content (C. Li, 2021).

Poisson's ratio relates lateral strain to axial strain in a rock sample under stress. It describes how much a material expands or contracts laterally when

compressed or stretched axially. Similar to the deformation modulus, it is typically calculated at 50% of the maximum strength:

$$\nu_i = -\frac{\Delta\epsilon_{r,50\%}}{\Delta\epsilon_{a,50\%}} \quad (2.9)$$

where ϵ_r is the lateral strain and ϵ_a is the axial strain. Typical values for intact rock range between 0.2 and 0.3 (C. Li, 2021).

2.1.2 Joint Properties

Unlike intact rock material, the rock mass is heterogeneous and often discontinuous. Rock mass refers to the in situ material consisting of intact rock blocks separated by discontinuities such as joints, faults, or other weakness zones, which together determine its mechanical behaviour. Joints refer to geological fractures in rock where no significant movement has occurred along the fracture surface (C. Li, 2021).

Figure 2.1.1 highlights important factors of the rock mass, including the degree of jointing (block size), determined by the joint pattern and orientation, and joint characteristics such as joint filling, length, alteration, and roughness. These characteristics play a significant role in influencing the shear strength of rock joints, which directly influences the overall strength of the rock mass. Additionally, the deformability of the rock mass depends on the stiffness of the joints, which is influenced by their mechanical properties. Discontinuities and their conditions generally weaken the rock mass, making it essential to consider them when designing support systems for underground excavations (C. Li, 2021).

As joint properties are of great importance and are also used in empirical methods, they will be introduced and explained in detail below.

The degree of jointing is determined by the joint spacing and orientation, making up the joint pattern. Joints typically occur in joint sets with approximately the same spacing between each other, and are typically easy to identify. Joint that does not appear in sets are often referred to as random joints (C. Li, 2021).

In fracture zones, the joint spacing is highly reduced, decreasing the stability. On the other hand, if the joint spacing is greater than the span or height of the excavation, the blocks will typically be too large to fall down. It is also worth noting that the degree of jointing is more important in hard rocks than soft rocks where deformation can occur independently of joints (*Using the Q-system 2022*).

The shear strength of joints depends on the surface conditions of the rock joint. One important factor is the joint roughness. It refers to the unevenness and waviness of the joint surface, which can be categorised into ten classes, each associated with a range of JRC (Joint Roughness Coefficient) values. This can be seen in Figure 2.1.3. The JRC is determined from shear testing and reflects the dilation angle i of the joint surface, ranging from 0° (smooth) to 20° (rough) (C. Li, 2021).

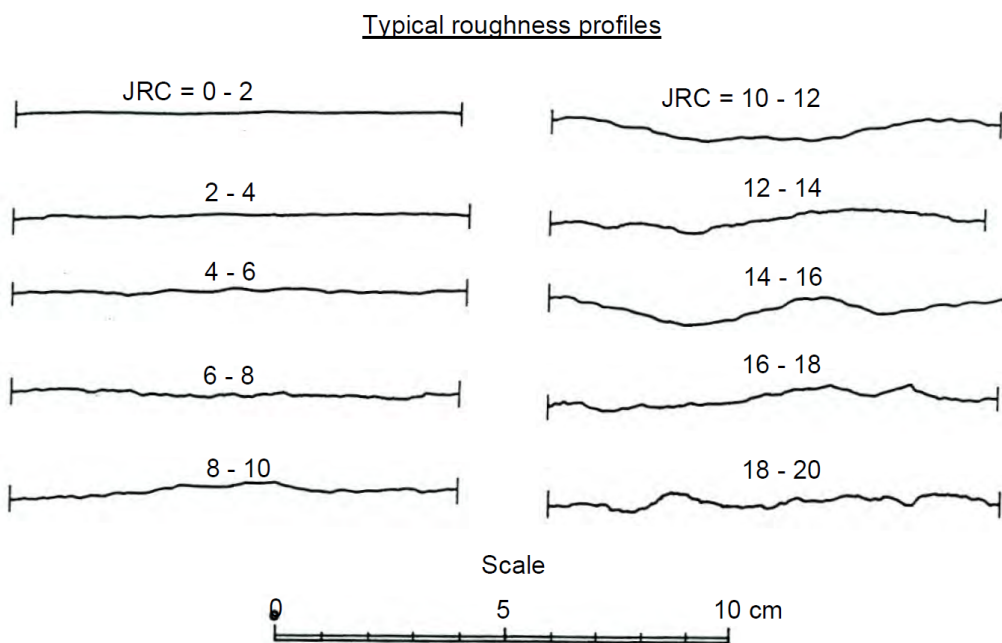


Figure 2.1.3: JRC (C. Li, 2021).

Roughness can also be described on two different scales. Small structures ranging from centimeters to millimeters on a joint surface are often characterised by terms such as rough, smooth, and slickensided. The other scale, ranging from decimeters to meters, describes the larger roughness of the joint, using terms like stepped, undulating, and planar. Rougher joints on

both scales, such as a rough stepped joint, provide the best shear strength. In contrast, a slickensided planar joint will result in lower shear strength (*Using the Q-system* 2022).

Joint alteration refers to the chemical or physical changes in a joint, such as weathering or the presence of filling materials, which affect its mechanical properties. The joint infill can vary in both thickness and strength, depending on its mineral composition. If the infill is thick enough, it can prevent rock wall contact and drastically reduce the shear strength and stiffness of the joint. The mineral composition also plays a critical role. Water can soften or wash out certain minerals, and swelling clays can further weaken the joint, both of which are unfavorable for shear strength (*Using the Q-system* 2022).

Joint separation is a term that can be compared to joint alteration. However, joint separation describes the distance between the joint surfaces without necessarily being filled with infill. The distance affects the interlocking (rock wall contact) ability of the surfaces and how much water and/or infill can occupy the space (Bieniawski, 1989).

The length, continuity, or persistence of a joint is important for the stability of an excavation. Longer and continuous joints are more significant than shorter joints that do not intersect the entire cross-section of the excavation. When a joint is very short, it is often referred to as a crack. These may have some local importance for smaller blocks but rarely affect larger blocks (*Using the Q-system* 2022).

As mentioned, water can have a drastic impact on the mineral fillings within a joint. If the water pressure in a joint is high enough, it can counteract the normal stress, σ_n , resulting in reduced shear strength. The water condition is usually described by the inflow rate, water pressure, and terms such as dry, damp/humid, dripping, or varying levels of inflow (*Using the Q-system* 2022).

Water inflow is not uncommon in underground excavations, and it can originate from the roof, walls, or invert. If the excavation is close to the surface, inflow may vary with the seasons, leading to quite different conditions. In some cases, the rock may be dry immediately after excavation but experience water inflow later. In other cases, there might be substantial water inflow initially, which decreases over time. Generally, water is considered a factor that negatively impacts stability, as it can weaken joints, reduce shear strength, and increase the need for drainage and support systems (*Using the Q-system*

2022).

To assess the shear strength of a joint, the direct shear test is commonly used. The specimen is secured in place with cement mortar or plaster, and an increasing shear force is applied parallel to the joint plane while maintaining a preset normal force perpendicular to the joint. Figure 2.1.4 illustrates this test. The results are plotted on a shear stress versus shear displacement curve. After the initial displacement, the joint has reached its peak shear strength. As displacement continues, the residual shear strength is observed, which is lower due to the smoothing of the joint surface (C. Li, 2021).

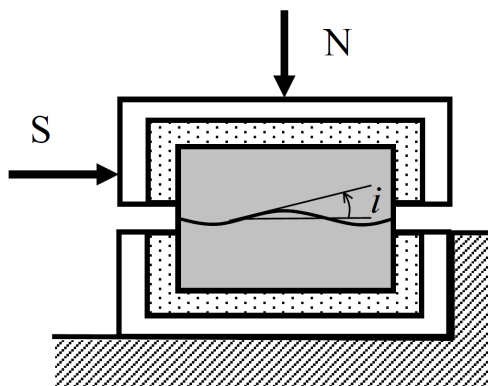


Figure 2.1.4: Direct shear test on a rock joint. N is the force normal to the joint, and S is the force parallel to the joint. The angle i is related to the apparent friction angle of the joint surface (C. Li, 2021).

The shear strength of a clean rock joint is linearly related to the normal stress applied to the joint and can be described by Coulombs law (C. Li, 2021):

$$\tau = \sigma_n \cdot \tan \phi \quad (2.10)$$

where σ_n is the normal stress, and ϕ is the apparent friction angle of the joint surface, expressed as $\phi = \phi_b + i$. Here, ϕ_b is the basic friction angle, a material constant measured using tilt tests, and i is the dilation angle that accounts for joint roughness (C. Li, 2021).

Joint stiffness refers to a joint's ability to resist normal deformation under applied stress. High stiffness results in less deformation, improving rock mass stability, while low stiffness allows greater deformation, reducing stability.

Measuring joint stiffness is challenging, but certain methods incorporate parameters like the deformation modulus to estimate it (C. Li, 2021).

Understanding how discontinuities impact the overall strength of a rock mass is crucial for accurate stability assessments and the design of support systems. Mechanical analysis of specimens with identified weakness planes is a key method for this purpose. By combining the mechanical properties of intact rock and the discontinuities in the rock mass, one can assess the true behaviour of the rock mass (Vásárhelyi and Kovács, 2017).

2.1.3 Rock Mass Design Parameters

Understanding and acquiring the main rock mass design parameters is of utmost importance for any engineering design in rock mass. Using intact rock properties directly on rock mass will, in most cases, yield highly unrealistic results and can result in a design not suited for the in situ conditions, jeopardizing both the project and worker safety. The discontinuities within the rock mass must be taken into account. Therefore, the intact rock properties must be reduced by an appropriate amount (Vásárhelyi and Kovács, 2017).

Figure 2.1.5 illustrates how the number and spacing of discontinuities, relative to the size of the structure under construction, influence the behaviour of the rock mass, resulting in properties that are quite different from those of intact rock.

The rock mass design parameters required for the design analysis depend on the methods used. Analytical and numerical methods require different parameters and also depend on whether the analysis is elastic, plastic, or another type. For plastic analysis in numerical modelling, residual values of Mohr-Coulomb parameters or Hoek-Brown parameters are necessary. In addition, information about dilation is required for some analysis (Vásárhelyi and Kovács, 2017). The Mohr-Coulomb and Hoek-Brown parameters will be presented in Sections 2.5.1 and 2.5.2, respectively.

Table 2.1.1 presents the most important rock mass design parameters used in underground excavation design. While all parameters listed are rock mass design parameters, they have been grouped for clarity. Note that all parameters are for rock mass, not intact rock. Water conditions and geometry are not included in the table but are also important factors to consider in the overall design process (C. Li, 2021).

Table 2.1.1: Presentation of Rock Mass Design Parameters

Rock Mass Design Parameters	Symbol
Basic Rock Mass Parameters	
Porosity	Φ
Unit Weight	γ
Compressive Strength	σ_{cm}
Tensile Strength	σ_{tm}
Poisson's Ratio	ν_m
Cohesion	c_m
Friction Angle	ϕ_m
Dilation	ψ
Dilation angle	i
Deformation Modulus	E_m
Shear Modulus	G_m
Residual Parameters	
Residual Compressive Strength	$\sigma_{cm,res}$
Residual Tensile Strength	$\sigma_{tm,res}$
Residual Cohesion	$c_{m,res}$
Residual Friction Angle	$\phi_{m,res}$
Residual Dilation	$\psi_{m,res}$
Residual Deformation Modulus	$E_{m,res}$
Residual Shear Modulus	$G_{m,res}$
Stresses	
Major principal stress	σ_1
Intermediate principal stress	σ_2
Minor principal stress	σ_3
Angle (Degrees from Horizontal)	θ

The different rock mass design parameters can be obtained through various methods. Empirical methods using classification and characterization systems can be used, as well as numerical modelling and in situ test. Some empirical equations for the estimation of key rock mass design parameters are presented later in Subsection 3.1.5. Methods involving numerical modelling and in situ testing will not be discussed further.

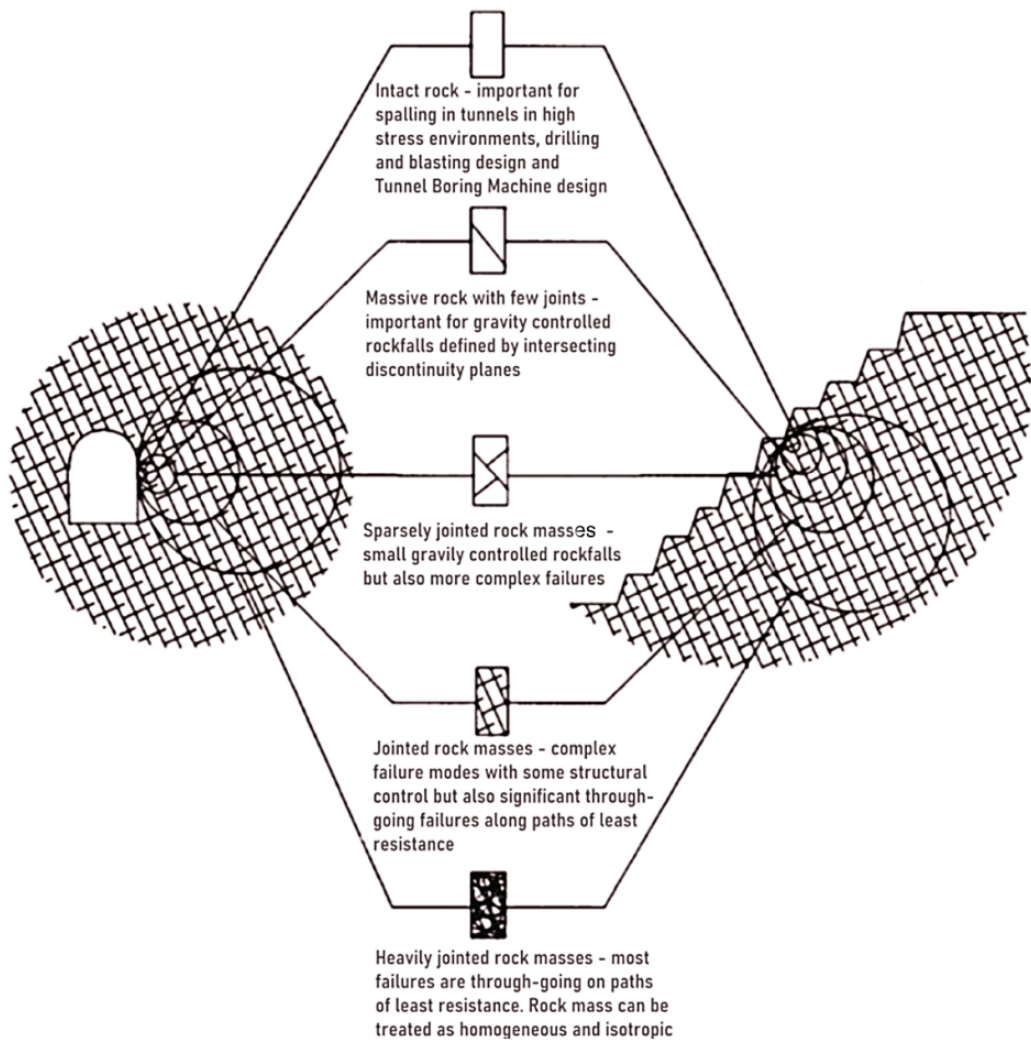


Figure 2.1.5: The influence of scale on jointed rock masses (Evert Hoek, 2007).

2.2 Stress Conditions

Understanding stress conditions at a given site is essential in both civil and mining industries, as the magnitude and direction of rock stresses significantly impact the stability of excavations and the development of effective support systems (Evert Hoek, 2007).

Rock stresses are primarily divided into two groups, in situ stresses and induced stresses. In situ stresses refer to the natural stresses present in the rock mass before any human activity, resulting from geological processes. Induced stresses, in contrast, are introduced by human activities like excavation, mining, and drilling, which can alter the natural balance and affect the stability of the rock mass (Evert Hoek, 2007).

Higher stress levels are often associated with rock failure. These stresses can also lead to deformations such as roof and sidewall closure, while tensile stresses may cause fractures that compromise block stability. Other stability issues under high stress conditions include floor heaving, spalling, squeezing, wall bulging, and rock bursts. Although high stresses can create challenging conditions, they may also contribute to excavation stability by tightly sealing discontinuities and keeping the rock mass dry (Evert Hoek, 2007).

Figure 2.2.1 illustrates the different categories of rock stresses and provides a visual summary of the subject.

This section provides an overview of the fundamental concepts of in situ and induced stresses, which are essential for analyzing stress-induced instability and designing support measures to stabilise the rock under these conditions.

In situ Stresses

The in situ stresses in a rock mass are the cumulative result of its geological history (Amadei and Stephansson, 1997). Predicting these stresses is challenging, partly due to frequent variations arising from the inhomogeneous and discontinuous nature of rock masses. Numerous methods for measuring in situ stresses are described by Amadei and Stephansson (1997). However, an estimate can still be obtained by applying the relationship between stress and depth.

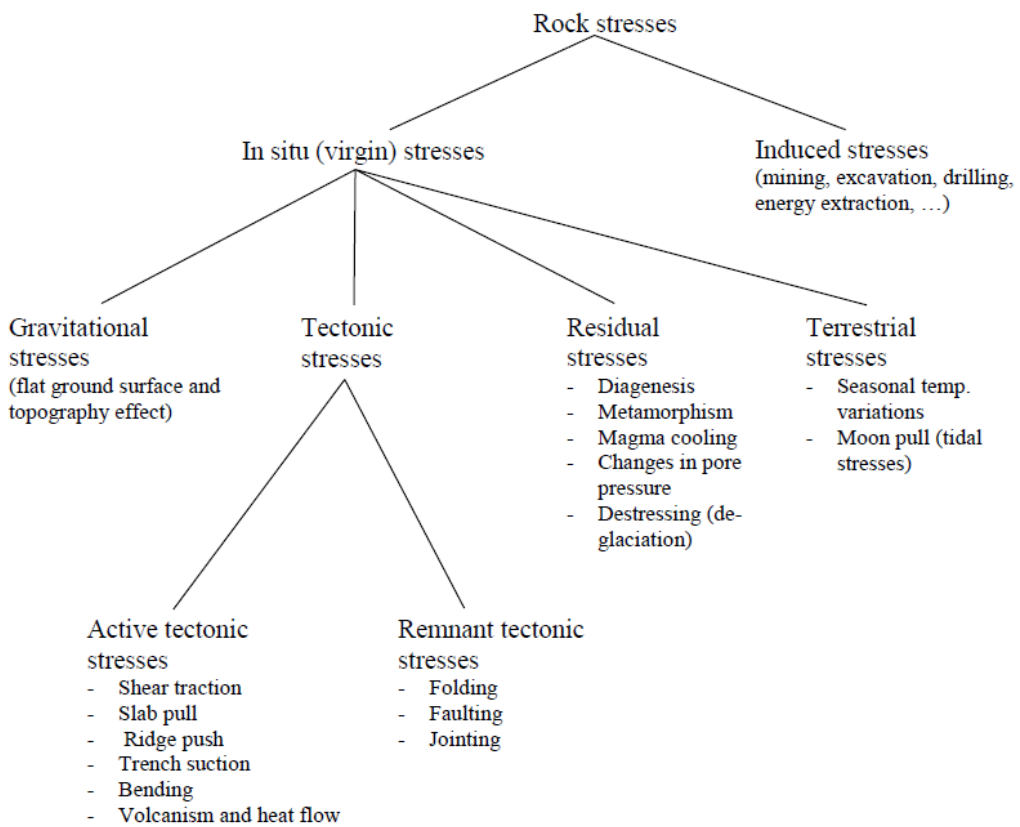


Figure 2.2.1: An overview of the stress terminology (Amadei and Stephansson, 1997).

When discussing the state of stress at depth z , it is common practice to divide it into two principal components: a vertical component, σ_z , and a horizontal component, σ_h (Amadei and Stephansson, 1997).

The vertical stress component is primarily caused by the weight of overlying rock (gravitational stress), making it increase linearly with the depth, statistically. The vertical stress, σ_v , is often calculated as:

$$\sigma_v = \rho \cdot g \cdot h \quad (2.11)$$

where ρ is the density of the overlying rock (kg/m^3), g is the gravitational acceleration (m/s^2), and h is the depth below surface (m) (Amadei and Stephansson, 1997).

It is common to assume a density of 2700 kg/m^3 , which allows the formula to be simplified to:

$$\sigma_v \approx 0.027 \cdot h \quad (2.12)$$

where σ_v is given in MPa and h in meters (Amadei and Stephansson, 1997).

This approach provides a reasonable estimate but is not always precise. In Figure 2.2.2, numerous vertical stress measurements are displayed in a scatter plot, with vertical stress in MPa on the x-axis and depth in meters on the y-axis. A linear trend line, based on Equation 2.12, is included for comparison. While a general trend is obvious, it is clear that the estimated line serves only as an approximation, as most data points fall outside the estimated line. This deviation is primarily due to local variations caused by geological features or active tectonic zones (Amadei and Stephansson, 1997).

The horizontal stress component is often challenging to estimate due to its complexity and the variety of influencing factors. Major contributors include tectonic stresses, which includes both active and remnant tectonic forces, as well as residual stresses and gravitational effects influenced by topography (Amadei and Stephansson, 1997).

Horizontal stresses can originate from a combination of these factors. Tectonic stresses are caused by large-scale forces acting on lithospheric plates, especially at plate boundaries. Residual, or "locked-in," stresses develop when loads are removed, such as during glacial melting, allowing the rock

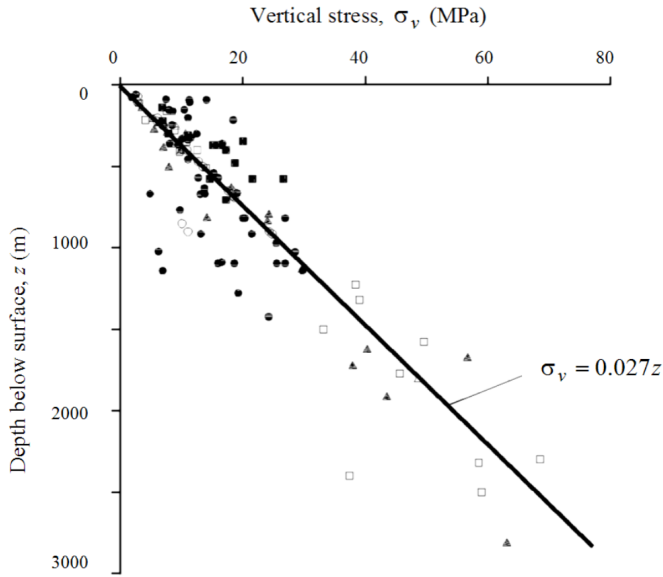


Figure 2.2.2: Vertical stress measurement around the world (C. Li, 2021).

to expand slightly. Geological structures like stratification, faults, and shear zones further affect stress distribution, often creating localised stress concentrations. In areas with steep topography, such as mountain slopes, valleys, and fjords, the largest principal stress tends to align parallel to the surface, which can lead to excavation challenges, including rockbursts, spalling, and fracturing (C. Li, 2021).

While high horizontal stresses can create challenging conditions, low horizontal stresses can also be problematic. From a stability perspective, a moderate level of horizontal stress is ideal. Excavations with large spans and low horizontal stress may face issues with rock falls, as there is little to hold the rock in place (Amadei and Stephansson, 1997).

The average horizontal stress to vertical stress is denoted as the factor k , expressed as:

$$\sigma_h = k \cdot \sigma_v = k \cdot \rho \cdot g \cdot h \quad (2.13)$$

k is not a constant value applicable to an entire area. It may vary depending on the rock fabric and the geological history of the rock mass. It is also likely to vary with depth and in different horizontal directions at a specific depth (Amadei and Stephansson, 1997).

In 1994, Sheorey presented an elasto-static thermal stress model of the Earth, providing a simplified equation for estimating the factor k :

$$k = 0.25 + 7 \cdot E_h \cdot \left(0.001 + \frac{1}{z}\right) \quad (2.14)$$

where m is the depth below the surface, and E_h (GPa) represents the average deformation modulus of the upper Earth's crust measured in the horizontal direction. This equation is illustrated in Figure 2.2.3 (Amadei and Stephansson, 1997), where E_h ranges from 10 to 100 GPa. The x-axis shows the factor k , and the y-axis represents depth in meters below the surface.

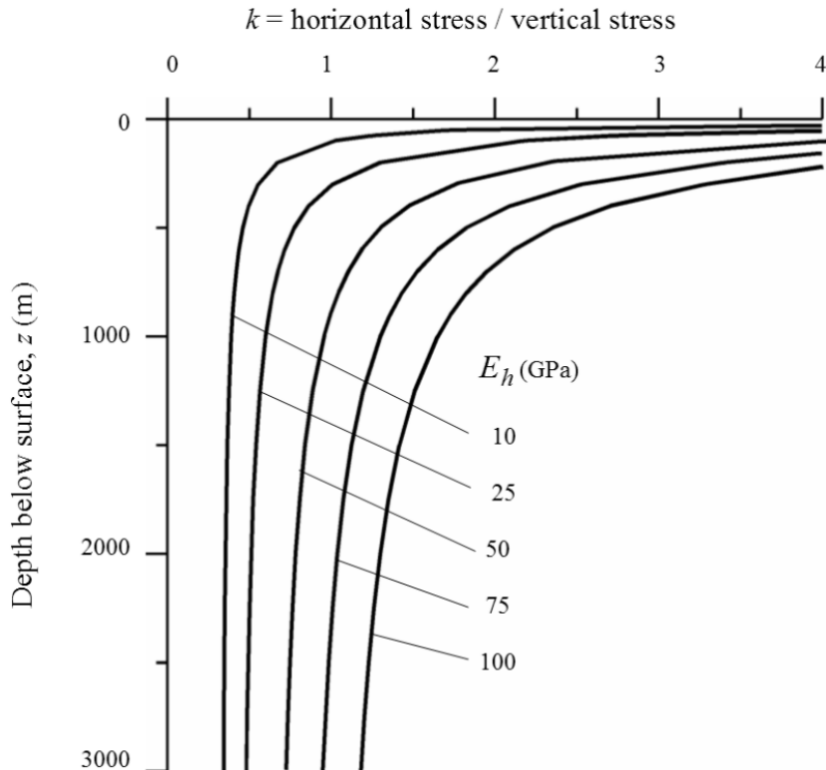


Figure 2.2.3: Relationship between depth and the ratio of horizontal to vertical stress k for different deformation moduli (E_h) based on Sheorey's equation (Evert Hoek, 2007).

Induced Stresses

Before an underground excavation begins, the in situ stress, consisting of σ_v , σ_{h1} , and σ_{h2} , is uniformly distributed within the rock mass, assuming the rock mass is both homogeneous and isotropic. During and after excavation, these stresses are redistributed as sections of the rock mass are removed. This will result in a change in both direction and magnitude of the stresses around the opening. As illustrated in Figure 2.2.4, the in situ stresses are redistributed around a circular opening. The largest principal stress, σ_h , aligns parallel to the periphery, while the smallest principal stress, σ_3 , is oriented perpendicular to the periphery. These stresses around an opening are referred to as tangential and radial stresses, respectively (Evert Hoek, 2007).

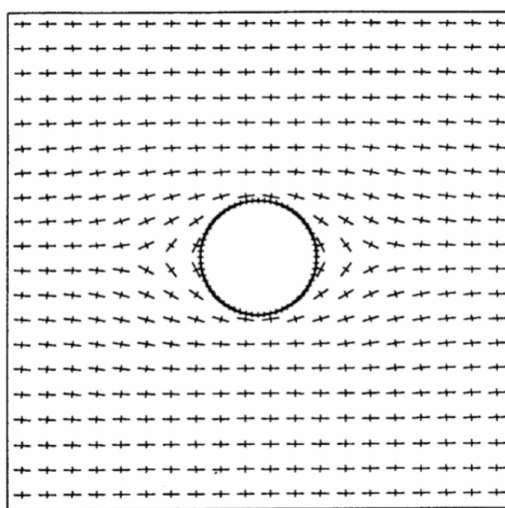


Figure 2.2.4: Illustration of stress redistribution around an excavation (Evert Hoek, 2007).

This change in the stress field can create areas of high stress (stress concentration) and low stress (stress relief). If not properly managed, high-stress zones can lead to ground failure mechanisms such as spalling, rockbursts or fracturing. Similarly, low-stress zones may result in loosening or instability, as there may be insufficient confinement to hold the rock mass in place. Effective design and support systems are essential to control these stress-induced failures and ensure the stability of the excavation (Evert Hoek, 2007).

The stress condition in rock masses is complex. Discontinuities, anisotropy, and heterogeneities within the rock can lead to complex stress regimes, while boundary conditions and topography may alter and rotate the in situ stresses. Additionally, phenomena beyond tectonic forces, such as local geological features, can result in high horizontal stresses, especially near the surface. Accurate stress measurements are crucial for designing support systems that address these varying conditions effectively.

One measure that can be taken to address challenging stress conditions is to adjust the geometry of the excavation to better accommodate the stress environment (C. Li, 2021). This last factor will be explained in the following section.

2.3 Geometry

Of the three primary factors in applied rock mechanics, geometry is the only one that can be altered and optimised to suit the conditions and intended use of the excavation. Different shapes, sizes, and orientations are suitable for different conditions, making it essential to have a thorough understanding of the other two factors: rock quality and stress condition. In general, smaller openings offer greater stability, and circular shapes are typically more stable than square ones. Other commonly used shapes include upright and horizontal ellipses, horseshoes, and combinations of these forms (Amadei and Stephansson, 1997).

Figure 2.3.1 illustrates various excavation shapes and the tangential stress concentrations in the roof and sides of a single opening placed in a uniform in situ stress field. The figure shows that openings with a horizontal main axis are better suited to conditions with higher horizontal stresses, while those with a vertical main axis are preferable when the vertical stress is greater (C. Li, 2021).

The quality of the rock mass significantly impacts the design of the excavation, particularly the dimensions of the opening. In high-quality rock masses, larger spans and heights can be achieved with minimal support, allowing for greater flexibility in excavation design. In contrast, poor-quality rock masses impose stricter limitations, as they require reduced spans and heights to maintain stability. Additional support elements are often necessary to stabilise weak or highly fractured rock. Ultimately, the excavation design must

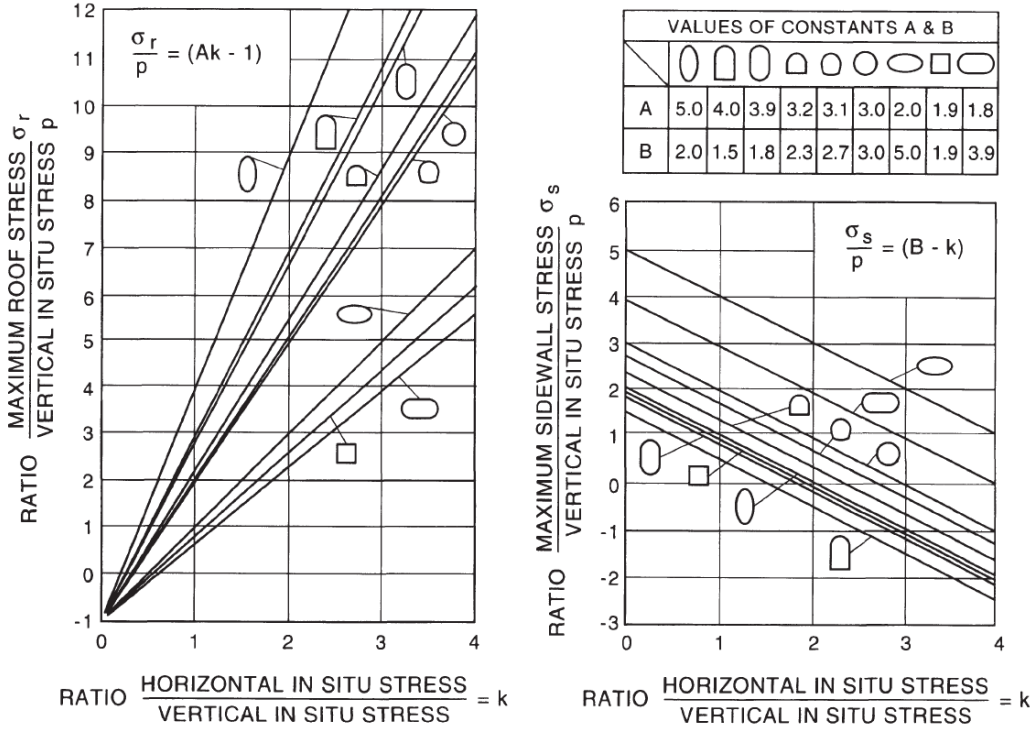


Figure 2.3.1: Stress concentrations around an excavation in a uniform stress field, with vertical and horizontal stress components. The rock mass is assumed to be homogeneous, continuous, and linearly elastic (C. Li, 2021).

balance the desired dimensions with the rock mass quality to ensure structural stability (C. Li, 2021).

Stress conditions are also essential to consider in excavation design. Both the distribution and magnitude of stresses determine the optimal shape, dimensions, and orientation of the excavation. The general goal is to minimise stress concentrations and create a uniformly distributed compressive environment around the opening, often referred to as the *harmonic hole* concept, while avoiding tensile stresses. Compressive stresses tend to concentrate in sharp corners, and with a larger excavation, a higher level of compressive and tensile stress is concentrated (Amadei and Stephansson, 1997).

The *harmonic hole* concept is effective when in situ stresses are low relative to rock strength. However, when stresses are high in comparison to rock strength, this approach may result in uniform but elevated stress levels around the opening, potentially leading to stability issues. In such cases, a possible solution is to concentrate stresses in sharp corners, thereby limiting

the extent of overstressed zones (Amadei and Stephansson, 1997).

The orientation of stresses relative to the excavation direction is, as mentioned, crucial for stability. This factor also depends on the magnitude of the stresses. At shallow depths, where horizontal stresses are low and the rock mass quality is fair to good, the drift should be oriented parallel to the smallest and perpendicular to the largest horizontal stress. In such low-stress regions, the largest horizontal stress can help compress the rock mass, enhancing stability in the roof (C. Li, 2021).

In higher-stress environments, however, it is not recommended to orient the drift perpendicular to the largest horizontal stress. This is because the additional compressive stress is not needed for stability and may, in fact, lead to stability problems (C. Li, 2021).

When considering stresses in excavation design, it is important to account for potential changes in stress conditions over time. This is particularly relevant in underground mining, where induced stresses from ongoing excavation activities can increase stress concentrations and lead to stability issues. Therefore, it is crucial to not only evaluate current stress levels but also anticipate future changes that may impact the excavation's stability (Amadei and Stephansson, 1997).

Perhaps the most critical factor in determining excavation geometry is the intended use of the space. The shape must be designed to fulfill its purpose, and the dimensions should be sufficient to accommodate its functional requirements without compromising stability. If these factors are not properly considered, the entire excavation or project may ultimately have little value (Amadei and Stephansson, 1997).

Once an appropriate geometry has been established, the next step is to prevent potential failures by implementing an effective rock stabilisation system tailored to the excavation's specific stress and rock mass conditions. The next section will cover the most widely used rock support elements and discuss their applications, advantages, and limitations in stabilizing underground excavations.

2.4 Rock Stabilisation Measures

After underground excavation activities, such as mining operations and civil engineering projects, a free rock surface is created. Stresses acting on the periphery can lead to de-stressed and overstressed rock masses, resulting in instabilities that require support. In de-stressed zones, wedges formed by discontinuities may fall. In overstressed zones, the rock may fail due to high ground pressure, leading to deformation or rockburst. Rock stability measures can be characterised into two groups: rock reinforcement and rock support (C. Li, 2021).

Rock reinforcement (or internal rock support) are stabilisation measures where the support device is installed within the rock mass itself. Popular examples are rockbolts and cable bolts (C. Li, 2021).

Rock support (or external rock support) are stabilisation measures where the devices are installed on the rock surface. The main goal is to stop rocks from falling, however some gives extra external support. Some examples are steel set, shotcrete arches, concrete lining, shotcrete liners, mesh, and lacing (C. Li, 2021).

Furthermore, these stabilisation measures will be introduced in a fundamental way to establish an overview of the most popular alternatives used in underground excavations.

2.4.1 Rock Reinforcement

Rockbolts are one of the most commonly used support devices in underground excavations, with each type of bolt serving a specific purpose (C. Li, 2021). They can be classified in various ways, with one effective approach being to organise them by both function and mechanism.

Functionally, rockbolts are divided into two main categories: conventional rockbolts and energy-absorbent (or yielding) rockbolts. Conventional rockbolts are generally designed for more static conditions with minimal dynamic loads, providing stability by preventing movement between rock layers. In contrast, energy-absorbent rockbolts are engineered to absorb deformation energy, making them suitable for environments with significant dynamic stresses, such as seismic zones or areas prone to rock bursts (C. Li, 2021).

Conventional rockbolts can be further categorised by mechanism into mechanical anchors, fully grouted bolts, and friction bolts.

Mechanical anchor bolts provide immediate support by expanding against the borehole walls to create a secure hold in the rock mass. One example is the expansion shell bolt, which has an expanding shell at its end that acts as an internal anchor. The external anchor is the face plate on the excavation surface, making it a two-point anchored bolt. The load capacity depends on the friction between the expansion shell and the rock mass, as well as the strength of the face plate. However, the anchor may lose stability if there are vibrations or if the rock mass quality is poor at the anchor point, reducing or even eliminating the bolt's function. Because of this, the load and deformation capacity can vary. While the bolt is known for a relatively low load capacity, its ability to take load immediately after a quick installation is a key advantage. Under pull loading, failure often occurs in the face plate, whereas under shear loading, it typically takes place in the bolt shank (C. Li, 2021).

Fully grouted rockbolts use resin grout or cement mortar to encapsulate the entire bolt length, bonding it securely to the borehole walls. The most widely used type, and an overall popular choice, is the fully grouted rebar bolt, which is essentially a rebar with a plate at the bolt head. With cement mortar, the bolt does not carry any load until after 24 hours. Resin grout, however, allows the bolt to bear load within seconds to 30 minutes, depending on the grout type. This bolt is known for its high load capacity and stiffness. Installation quality is reliable, and the bolt is also protected against corrosion. One disadvantage, however, is that the bolt has limited deformation capacity. Failure typically occurs in the bolt shank under both pull and shear loading (C. Li, 2021).

The final category of conventional rockbolts, friction bolts, relies on friction between the bolt and the surrounding rock mass along the entire bolt length. Examples include Split Set and Swellex bolts. While their performance characteristics differ slightly, friction bolts are generally known for their low load capacity but can accommodate large rock deformations. They begin carrying load immediately after installation, which typically takes only 2–5 minutes. In addition to their low load capacity, other disadvantages include susceptibility to corrosion and low shear strength. Both the Split Set and Swellex bolts fail within the bolt steel under shear loading and have a higher shear load capacity than pull load capacity (C. Li, 2021).

The other main category, energy-absorbent bolts, is a more recent innovation designed for use in high-stress conditions. These bolts are particularly effective in managing energy release from rockbursts in hard rock and rock squeezing in weaker rock following excavation. The bolts must be strong enough to withstand high stresses while also having the capacity to deform under load, absorbing energy from the rock. Most importantly, the bolt must maintain its integrity without failing under these challenging conditions. A common feature of these bolts is that they have a smooth bar and use cement mortar or resin grout, however, their anchoring mechanisms differ. Examples of these bolts include the D-bolt, Cone bolt, Yield-Lok, and Garford bolt (C. Li, 2021).

The D-bolt uses multiple small anchors along its length to bond to the grout, while the smooth bar between the anchors deforms to absorb energy released by the rock. Its load capacity is comparable to that of a fully grouted rebar bolt, but it has significantly greater deformation capacity. Even if one section of the bar fails, the rest of the bolt will continue to reinforce the rock mass (C. Li, 2021).

The other energy-absorbent bolts mentioned are two-anchor bolts, with one anchor at the end of the bolt and the other as the face plate. The cone bolt has a cone anchor at its end. As the rock deforms, the bolt moves along with it, and the cone is pulled through the resin, absorbing energy. The Yield-Lok operates on a similar principle, with its anchor encapsulated in a polymer material. When the bolt reaches its maximum pre-set load, the polymer remains in place while the bolt moves with the face plate, allowing deformation. The Garford bolt, has a resin-encapsulated anchor that allows the bolt to be pulled through under a pre-set load as the rock expands, thus absorbing energy and preventing failure (C. Li, 2021).

Another type of internal rock support is the cable bolt, used in situations where the rock mass needs stabilization over greater lengths. Typical cable bolt lengths in underground excavations range from 5 to 30 meters, but they can reach up to 100 meters when used for slope stability. Unlike conventional bolts made from solid steel bars, cable bolts consist of multiple strands twisted together. They are encapsulated in grout or resin, and sections of the cable can be de-bonded to enhance deformability. Cable bolts are known for their high load capacity and ease of handling. However, one drawback is their high stiffness, which limits their deformability (C. Li, 2021).

2.4.2 Rock Support

Sprayed concrete, commonly known as shotcrete, has become a popular choice in both mining operations and civil engineering projects over the last few decades. It is composed of cement, sand, fine aggregate, fibers, and water, which are mixed and sprayed onto the rock surface. Fiber-reinforced shotcrete has become standard practice, as it is tougher than plain shotcrete. However, if the rock undergoes significant deformation, the shotcrete may crack, creating an unsafe working environment. One solution to this is to apply mesh on the outside of the shotcrete layer. Another method is to embed the mesh within the shotcrete, which provides greater load-bearing capacity but is less able to deform than mesh applied externally. Shotcrete is capable of providing rapid support, depending on the composition of the mixture (C. Li, 2021).

The primary function of mesh in underground excavations is to restrain loose rock from falling. Two popular types are welded mesh and chain-linked mesh. Welded mesh is stiffer, while chain-linked mesh has a much greater deflection capacity. Both types are secured with rock bolts, and the wire diameter, grid size, and sheet dimensions can vary based on specific requirements. As mentioned in the previous section, mesh can be used in combination with shotcrete and rock bolts to enhance stability (C. Li, 2021).

Another reinforcement option is the mesh strap, typically made of welded steel wires. These straps are much longer than they are wide and are often positioned over shotcrete or mesh sheets to further stabilise the rock mass. They are also secured in place with bolts (C. Li, 2021).

Arches, such as steel sets and shotcrete arches, provide additional external support and are primarily used in extremely poor rock conditions. The poorer the rock quality, the closer the spacing of the arches should be. They should also be positioned close enough to interact structurally without excessive gaps that reduce their effectiveness (C. Li, 2021).

Steel sets are the more traditional of the two and have a long history in both mining and civil engineering. They are typically constructed from U- or I-shaped steel beams. A drawback of steel sets is their limited deformation capacity before failure. To address this, yielding elements or frictional sliding joints can be incorporated to increase flexibility (C. Li, 2021).

Shotcrete arches are a more cost-effective and simpler alternative to steel

sets. They are constructed using rock bolts, steel ribs, and shotcrete. Like steel sets, shotcrete arches have limited deformation capacity before failure. One solution is to delay the installation of shotcrete arches until after initial rock deformation has occurred (C. Li, 2021).

2.5 Failure Criteria

One of the most crucial aspects of rock engineering is rock failure. During excavation, it is often desirable for some rock to fail in a controlled manner, while after the excavation is completed, the remaining rock mass should remain stable and avoid failure (Labuz and Zang, 2015).

To achieve this, an accurate assessment of rock mass strength is necessary. When the stress condition reaches the ultimate strength, this is referred to as the *failure criterion*. It is common to use the principal stresses σ_1 , σ_2 , and σ_3 in these criteria, where the convention is positive for compression and negative for tension. It is also implied that failure is expressed in terms of effective stress (Labuz and Zang, 2015).

Choosing the most suitable failure criterion for a rock excavation project can be challenging. Multiple criteria are available, each based on different theories and empirical data from various conditions. However, the two most widely adopted failure criteria in rock engineering are the Mohr-Coulomb failure criterion and the Hoek-Brown failure criterion (Labuz and Zang, 2015).

Although both criteria neglect the intermediate principal stress (σ_2), they differ significantly in approach: Mohr-Coulomb is linear, while Hoek-Brown is non-linear, with each criterion offering its own advantages and disadvantages (Labuz and Zang, 2015).

The Mohr-Coulomb and Hoek-Brown failure criteria will be presented in the following section.

2.5.1 Mohr-Coulomb Failure Criterion

The Mohr-Coulomb (MC) failure criterion is a linear model for defining the conditions that lead to failure in isotropic materials. It proposes that failure occurs when there is a specific balance between the forces pushing against

a potential failure plane (normal stresses) and the forces causing it to slide (shear stresses). This criterion combines the foundational work done by Coulomb and Mohr (Labuz and Zang, 2015).

History

The origins of the criterion trace back to the work of Coulomb in 1776, a French military officer, physicist, and engineer. Coulomb proposed a linear relationship between shear stress (τ) and normal stress (σ_n), forming a linear failure envelope. According to his theory, specific combinations of these stresses will lead to failure along a plane within the material (Labuz and Zang, 2015).

Mohr was a German civil engineer, known for his contributions to structural engineering, including the development of Mohr's circle. Mohr expanded on Coulomb's work in the early 1900's, assuming that failure only is effected by σ_1 and σ_3 , and that the failure envelope could be either linear or non-linear (Labuz and Zang, 2015).

Mohr's circle provides a visual representation of the major (σ_1) and minor (σ_3) principal stresses on a σ - τ plot. The intermediate principal stress (σ_2) is therefore neglected. The circle is constructed by plotting these principal stress values from multiple triaxial tests with different confining pressures (σ_3) along the x-axis, then drawing circles through each set of points corresponding to σ_1 and σ_3 . By drawing a line that is tangent to all these circles, the failure envelope is created, representing the critical stress states that lead to failure. For compressive loading, the failure envelope is shown in Figure 2.5.1. To construct Mohr's circle under tensile stress conditions, a Brazilian tensile test or a direct tensile strength test should be performed (Labuz and Zang, 2015).

Formulas and parameters

According to the MC criterion, shear failure is described by (C. Li, 2021):

$$\tau = c + \sigma_n \cdot \tan(\phi) \quad (2.15)$$

where τ represents the shear stress, c the cohesion, σ_n the normal stress

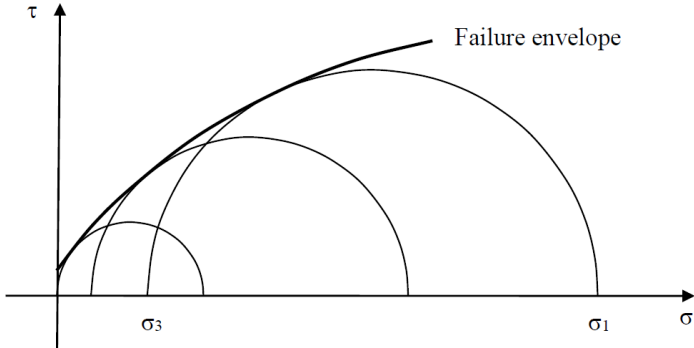


Figure 2.5.1: Non-linear failure envelope derived from multiple Mohr's circles (C. Li, 2021).

and ϕ the internal friction angle (C. Li, 2021). An illustration of the linear criterion, based of two Mohr circles, is presented in Figure 2.5.3.

Equation 2.15 can be applied to intact rock, discontinuities, and rock mass. However, the parameters used in the failure criterion must be carefully determined for each specific case. For intact rock failure, the parameters should reflect the properties of the intact rock. For discontinuities, the values must represent the characteristics of the discontinuity. In the case of rock mass failure, rock mass parameters accounting for its overall structure and properties must be used. The failure criterion for rock mass is then expressed as:

$$\tau_f = c_m + \sigma'_n \tan(\phi_m) \quad (2.16)$$

Here, τ_f is the shear strength of the rock mass, c_m is the rock mass cohesion, σ'_n is the effective normal stress, and ϕ_m is the internal friction angle of the rock mass.

As mentioned in Section 2.1, rock samples in compression tests typically undergo shear failure, resulting in one or two conjugate fractures. To describe the orientation of the fracture plane, the angles α and θ are used, both referred to as *fracture angle*. The relationship between α , θ and ϕ can be expressed as (C. Li, 2021):

$$\beta = \frac{\pi}{4} + \frac{\phi}{2} \quad \text{or} \quad \theta = \frac{\pi}{4} - \frac{\phi}{2} \quad (2.17)$$

It is also worth noting that the MC criterion relies on the *effective shear stress*, which accounts for the frictional resistance on the failure plane, not the *absolute shear stress*. The effective shear stress reaches its maximum when $\beta = (\frac{\pi}{4} + \frac{\phi}{2})$, which is also the angle at which shear stress failure occurs. The minimum effective shear stress is at $\beta = 45^\circ$ (C. Li, 2021).

Expressing τ and σ_n in terms of σ_1 and σ_3 , we can write the Mohr-Coulomb failure criterion as (C. Li, 2021):

$$\sigma_1 = \frac{1 + \sin \phi}{1 - \sin \phi} \sigma_3 + \frac{2c \cos \phi}{1 - \sin \phi} \quad (2.18)$$

Letting

$$k = \tan^2 \left(\frac{\pi}{4} + \frac{\phi}{2} \right) \quad (2.19)$$

the MC criterion can also be expressed as (C. Li, 2021):

$$\sigma_1 = k\sigma_3 + 2c\sqrt{k} \quad (2.20)$$

In a UCS test, σ_3 is set to 0, allowing the uniaxial compressive strength (σ_c) to be expressed in terms of c and ϕ (C. Li, 2021):

$$\sigma_c = 2c \tan \left(\frac{\pi}{4} + \frac{\phi}{2} \right) \quad (2.21)$$

In the presence of pore pressure (p), the principal stresses σ_1 and σ_3 must be substituted with their effective values, represented as $(\sigma - p)$ (C. Li, 2021).

$$(\sigma_1 - p) = k(\sigma_3 - p) + 2c\sqrt{k} \quad (2.22)$$

Figure 2.5.2, presents the MC failure criterion by Equation 2.15 and Equation 2.20 in two different coordinate systems.

The linear envelope (shown in Figure 2.5.3) is most accurate under compressive stresses, especially when the uniaxial compressive strength is much

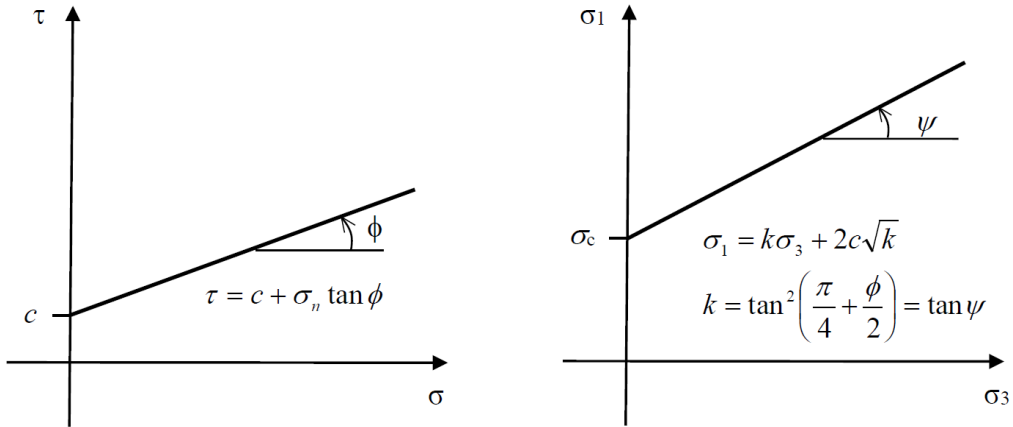


Figure 2.5.2: MC failure criterion illustrated in both τ - σ (left) and σ_1 - σ_3 (right) coordinate systems (C. Li, 2021).

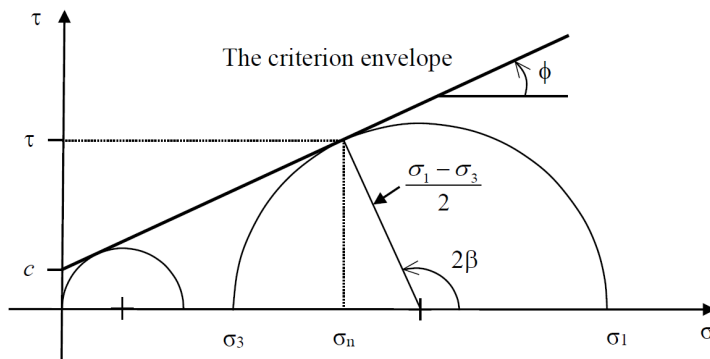


Figure 2.5.3: Illustration of the linear MC criterion using Mohr's circle, shown for both UCS and triaxial test conditions (C. Li, 2021).

greater than the uniaxial tensile strength σ_t . When tensile stresses are involved, modifications are often necessary, as the MC criterion does not perfectly predict the uniaxial tensile strength, which cannot always be matched in experiments. Therefore, when $\sigma < 0$, a simple extrapolation is usually done in the tensile region (Labuz and Zang, 2015).

The MC criterion has proven effective in many practical applications due to its simplicity and linearity, yet Mohr's model also allowed for a curved failure envelope to reflect the non-linear behaviour exhibited by certain rock types. It is recommended to use the MC criterion when dealing with compressive stresses within a limited range of mean stress (Labuz and Zang, 2015).

2.5.2 Hoek-Brown Failure Criterion

The Hoek-Brown criterion is a widely used failure criterion that provides a more advanced approach to assessing the strength of massive and jointed rock masses. Unlike the MC criterion, it accounts for the complex behaviour of fractured rock, making it essential in modern rock mechanics design for underground excavations and slopes. The criterion was empirically derived from triaxial tests, to describe a non-linear increase of peak strength of isotropic rock with increasing confining stress (Labuz and Zang, 2015). This section will cover the development, evolution, theory, and practical applications of the Hoek-Brown criterion, including its integration with the Geological Strength Index (GSI). A more detailed explanation of the GSI system is provided in Section 3.1.4.

History

The Hoek-Brown failure criterion was introduced in 1980 to provide input data for designing underground excavations in rock masses. At the time, no similar methods were available, so the main objective was to create a dimensionless equation adaptable to geological data. While the equation itself was not new, as it had been used to describe concrete failure since 1936, the connection to geological observations was innovative. Since then, numerous updates and revised versions have been published, aiming to improve the criterion's applicability and accuracy (Hoek and P. Marinos, 2007).

Early in the criterion's development, Hoek and Brown realised that it would be practically useless unless the parameters could be estimated quickly and easily in the field. Since the RMR system was already widely used, they proposed in 1988 to use RMR as the primary source of geological input, rather than creating a new classification system (Hoek and P. Marinos, 2007).

In 1992, a revised version of the original failure criterion introduced a new parameter, a , which altered the curvature of the failure envelope. This modification addressed the criterion's application to very poor-quality rock masses, which differ significantly from the hard rock masses the criterion was originally designed for (Hoek and P. Marinos, 2007).

By 1994, the Hoek-Brown failure criterion was further refined with the development of the *generalised Hoek-Brown criterion*, combining previous versions

to better suit a range of rock qualities. The generalised criterion applied the original Hoek-Brown model for rock masses with RMR values greater than 25 and the modified version for those with RMR values below 25, which represent poorer rock masses (Hoek and P. Marinos, 2007).

Around the same time, the Geological Strength Index (GSI) was introduced to address limitations in using RMR for very poor-quality rock masses. Unlike RMR, which relies on quantitative data, GSI is based on fundamental geological observations, allowing for a more qualitative assessment of the rock masses (Hoek and P. Marinos, 2007).

In 1998, a new GSI chart was published to complement the existing chart from 1994, which was primarily suited for better-quality rock masses. The new chart was designed specifically for very poor-quality rock masses (Hoek and P. Marinos, 2007).

A major re-evaluation of the Hoek-Brown criterion occurred in 2002, refining the relationships between parameters m , s , a , and GSI. Additionally, the disturbance factor D , accounting for blast damage, was introduced. The RocLab software was also released, providing an accessible tool for implementing the Hoek-Brown criterion. The 2002 update also explored the relationship between the Hoek-Brown and MC criteria, establishing equations for applying the criterion to slopes and underground excavations (Hoek and P. Marinos, 2007).

Later publications have expanded on the application of the GSI chart to various geological conditions, and additional GSI charts have been developed. Among these is a chart specifically designed for heterogeneous rock masses, such as flysch, and another for quantifying GSI based on joint condition $JCond_{89}$, and RQD. The basic GSI chart commonly used today was published in 2002 (Hoek and P. Marinos, 2007), and is presented in Figure 3.1.3.

Formulas and parameters

Following numerous triaxial tests on rock samples, an empirical equation was proposed to describe the failure of intact rock mass under different stress conditions (E. Hoek and Brown, 2019):

$$\sigma_1 = \sigma_3 + \sigma_{ci} \cdot \sqrt{m_i \cdot \frac{\sigma_3}{\sigma_{ci}} + 1} \quad (2.23)$$

where σ_1 and σ_3 are the major and minor principal stresses, σ_{ci} represents the unconfined compressive strength (E. Hoek and Brown, 2019), and m_i is a material constant related to the frictional properties of the intact rock (P. Marinos and Evert Hoek, n.d.).

The generalised Hoek-Brown failure criterion was introduced in 1994 to model the failure of highly fractured rock masses as a continuum, due to the high density of discontinuities. This failure criterion is expressed as (E. Hoek and Brown, 2019):

$$\sigma_1 = \sigma_3 + \sigma_{ci} \cdot \left(m_b \cdot \frac{\sigma_3}{\sigma_{ci}} + s \right)^a \quad (2.24)$$

where m_b , s and a are the rock mass material constants given by (E. Hoek and Brown, 2019):

$$m_b = m_i \cdot \exp \left(\frac{GSI - 100}{28 - 14 \cdot D} \right) \quad (2.25)$$

$$s = \exp \left(\frac{GSI - 100}{9 - 3 \cdot D} \right) \quad (2.26)$$

$$a = \frac{1}{2} + \frac{1}{6} \cdot (e^{-GSI/15} - e^{-20/3}) \quad (2.27)$$

D represents the level of disturbance in the rock mass, influenced by blasting impacts and reduction in stress. D ranges from 0 to 1 and can be chosen from a table provided by E. Hoek and Brown (2019), including both pictures and a description of the rock mass. Note that when a is set to 0.5, s to 1, and m_b equals m_i , the original Hoek-Brown failure criterion for intact rock is obtained.

Figure 2.5.4 provides a visual representation of the relationship between the Hoek–Brown failure envelope for intact rock and the adjustments made for rock mass strength using the Geological Strength Index (GSI) and the disturbance factor D .

The equations for the new parameters introduced in the generalised version were designed to address rock masses composed of interlocking angular blocks, where failure occurs due to sliding and rotation rather than intact rock failure, particularly under low to moderate confining stress.

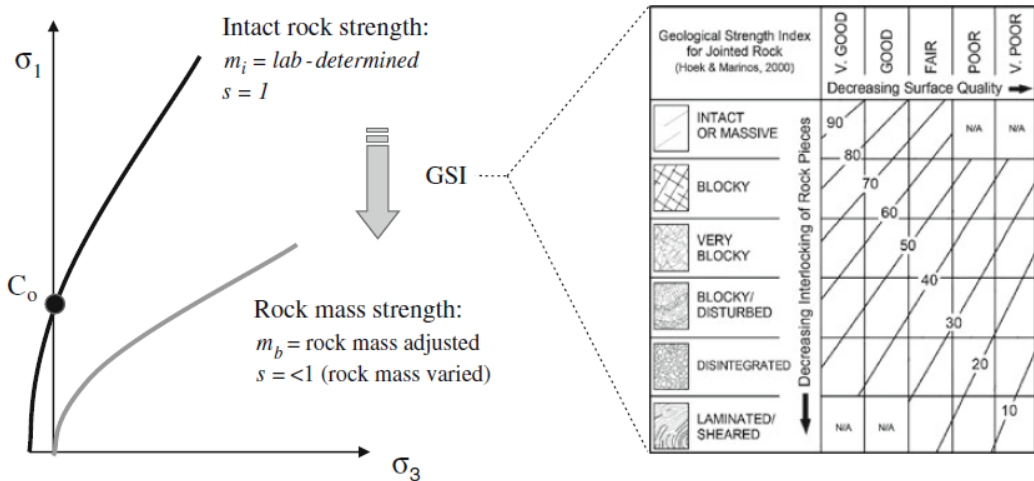


Figure 2.5.4: Adjusting the Hoek–Brown failure envelope from intact rock to rock mass strength using GSI and D (Labuz and Zang, 2015).

As explained earlier in this subsection, the two different Hoek–Brown failure criteria are applied based on rock mass conditions. The original Hoek–Brown criterion is used for intact rock, with parameters derived from lab tests, while the generalised Hoek–Brown criterion with GSI is suited for fractured or jointed rock masses, accounting for structure and surface conditions. Figure 2.5.5 illustrates this transition.

The unconfined compressive strength, together with the material constant m_i , should be determined by triaxial tests in a laboratory, as this provides the most accurate and reliable values. Evert Hoek (2007) recommends using at least five well-spaced data points from triaxial tests, as well as following the same interval used by Evert Hoek (2007): $0 < \sigma'_3 < 0.5 \cdot \sigma_{ci}$. It is also noted that the tests should be conducted at moisture levels similar to field conditions, as increased moisture content can often lead to a decrease in strength (Evert Hoek, 2007).

After the necessary tests have been successfully completed and data collected, the results can be analysed to determine the required constants for the intact rock mass, including the uniaxial compressive strength σ_{ci} , the Hoek–Brown constant m_i and the coefficient of determination r^2 (Evert Hoek, 2007).

The analysis is usually done by software like RocLab, and will not be explained further. However, when triaxial tests are not available, Table 2.5.1 and Table 2.5.2 can be used to estimate the constants.

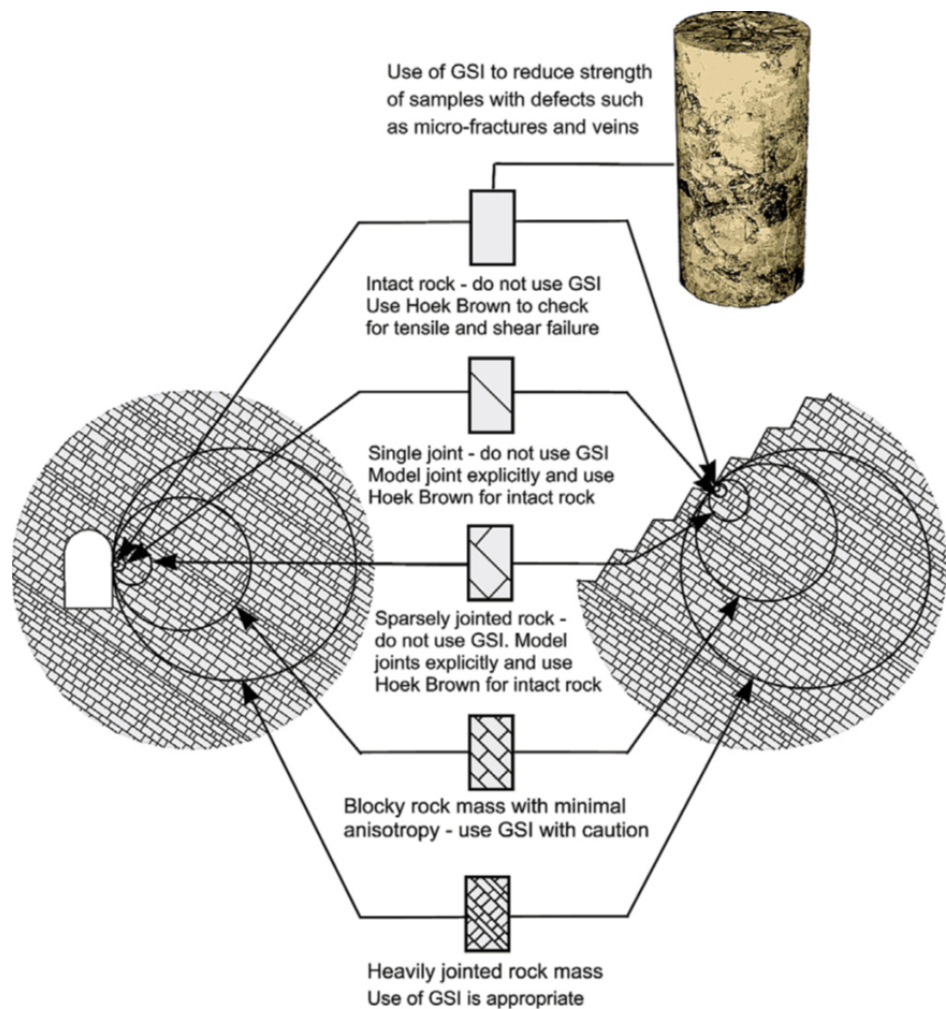


Figure 2.5.5: Choice of failure criterion depends on the size and characteristics of the rock mass (E. Hoek and Brown, 2019).

Figure 2.5.6 illustrates the overall design process when using the generalised Hoek-Brown failure criterion and the GSI system. The flowchart demonstrates how laboratory data is combined with field observations and estimates to calculate the principal stress relationship for the rock mass. These findings are then used to develop an excavation design through analytical or numerical methods. Once the excavation design is implemented, its performance is monitored using displacement measurements (E. Hoek and Brown, 2019).

The final step in this process is back analysis. Displacement monitoring provides direct insight into how the rock mass responds to the implemented design. This allows engineers to validate the input parameters used in the excavation design and iteratively adjust the input parameters and design as the project progresses (E. Hoek and Brown, 2019).

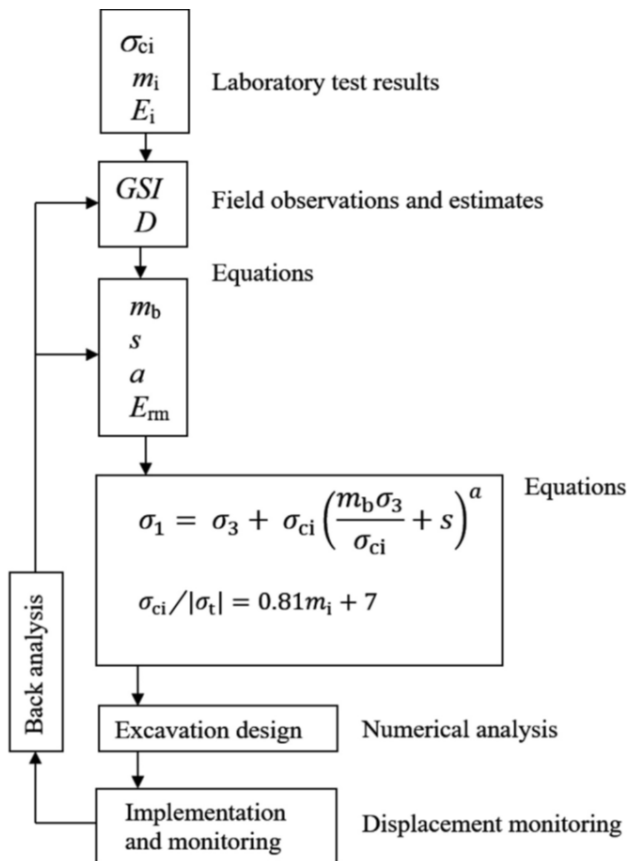


Figure 2.5.6: Flowchart for using the Generalised Hoek-Brown criterion and GSI in excavation design (E. Hoek and Brown, 2019).

Grade*	Term	Uniaxial Comp. Strength (MPa)	Point Load Index (MPa)	Field estimate of strength	Examples
R6	Extremely Strong	> 250	>10	Specimen can only be chipped with a geological hammer	Fresh basalt, chert, diabase, gneiss, granite, quartzite
R5	Very strong	100 - 250	4 - 10	Specimen requires many blows of a geological hammer to fracture it	Amphibolite, sandstone, basalt, gabbro, gneiss, granodiorite, limestone, marble, rhyolite, tuff
R4	Strong	50 - 100	2 - 4	Specimen requires more than one blow of a geological hammer to fracture it	Limestone, marble, phyllite, sandstone, schist, shale
R3	Medium strong	25 - 50	1 - 2	Cannot be scraped or peeled with a pocket knife, specimen can be fractured with a single blow from a geological hammer	Claystone, coal, concrete, schist, shale, siltstone
R2	Weak	5 - 25	**	Can be peeled with a pocket knife with difficulty, shallow indentation made by firm blow with point of a geological hammer	Chalk, rocksalt, potash
R1	Very weak	1 - 5	**	Crumbles under firm blows with point of a geological hammer, can be peeled by a pocket knife	Highly weathered or altered rock
R0	Extremely weak	0.25 - 1	**	Indented by thumbnail	Stiff fault gouge

* Grade according to Brown (1981).

** Point load tests on rocks with a uniaxial compressive strength below 25 MPa are likely to yield highly ambiguous results.

Table 2.5.1: Field estimates of uniaxial compressive strength (Evert Hoek, 2007).

Rock type	Class	Group	Texture			
			Coarse	Medium	Fine	Very fine
SEDIMENTARY	Clastic		Conglomerates*	Sandstones (21 ± 3)	Siltstones 17 ± 4	Claystones 7 ± 2
			Breccias (19 ± 5)		Greywackes (18 ± 3)	Shales 4 ± 2
						Marls (6 ± 2)
	Non-Clastic	Carbonates	Crystalline Limestone (12 ± 3)	Sparitic Limestones (10 ± 2)	Micritic Limestones (9 ± 2)	Dolomites (9 ± 3)
		Evaporites		Gypsum 8 ± 2	Anhydrite 12 ± 2	
		Organic				Chalk 7 ± 2
	Metamorphic	Non Foliated	Marble 9 ± 3	Hornfels (19 ± 4)	Quartzites 20 ± 3	
				Metasandstone (19 ± 3)		
		Slightly foliated	Migmatite (29 ± 3)	Amphibolites 26 ± 6		
IGNEOUS	Plutonic	Light	Granite 32 ± 3	Diorite 25 ± 5		
				Granodiorite (29 ± 3)		
		Dark	Gabbro 27 ± 3	Dolerite (16 ± 5)		
	Hypabyssal		Norite 20 ± 5			
					Diabase (15 ± 5)	Peridotite (25 ± 5)
	Volcanic	Lava		Rhyolite (25 ± 5)	Dacite (25 ± 3)	Obsidian (19 ± 3)
		Pyroclastic	Agglomerate (19 ± 3)	Breccia (19 ± 5)	Tuff (13 ± 5)	

* Conglomerates and breccias may present a wide range of m_i values depending on the nature of the cementing material and the degree of cementation, so they may range from values similar to sandstone to values used for fine grained sediments.

**These values are for intact rock specimens tested normal to bedding or foliation. The value of m_i will be significantly different if failure occurs along a weakness plane.

Table 2.5.2: Estimated values for m_i by rock group (Evert Hoek, 2007).

Chapter 3

Support Design Methodologies

There are different methods one can use in the process of designing support systems for underground excavations. The oldest methods are experience-based and empirical methods, developed from data gathered across various projects. These are easy and quick to use, providing a useful starting point for support design. However, they have significant limitations, and on their own, they are often insufficient for creating an optimized support system. Analytical methods, based on mathematical formulations, can provide insights into the interaction between the rock mass and the applied support. These methods are valuable but rely on simplified conditions that often does not fully represent reality. Numerical modelling, on the other hand, overcomes many of these simplifications. It can estimate stresses and deformations in both 2D and 3D, accounting for complex conditions, making it an essential tool for achieving an optimized support design (Evert Hoek, 2007).

This chapter introduces all three approaches: empirical methods, analytical methods, and numerical modelling. It discusses their principles, applications, and limitations, providing a comprehensive understanding of how these methods can be used individually or, preferably, in combination to design effective support systems for underground excavations.

3.1 Empirical Design Methods

Empirical methods utilise characterization and classification systems to provide recommendations for appropriate support measures.

Rock mass classification involves assigning a rating or quality to a rock mass based on its material and structural properties (Abbas and Konietzky, 2015). The classification systems use empirical correlations between rock mass parameters and the behaviour of the rock under various conditions (Singh and Goel, 1999). This approach allows engineers to use experience from other sites regarding rock conditions, support needs, and stope design for the conditions expected at their own site (Abbas and Konietzky, 2015).

These classification systems form the foundation of empirical design methods within rock engineering, and have been successfully adopted worldwide. When used as intended, the systems play a critical role, particularly during the feasibility design stage, offering valuable insight into rock mass behaviour and the support requirements for underground excavations (Singh and Goel, 1999). These systems are highly regarded for their simplicity and their ability to handle uncertainties in complex geological conditions.

Singh and Goel (1999) mention four reasons why the quantitative rock mass classification systems have been so successful:

- (i) It provides better communication between geologists, designers, contractors and engineers;
- (ii) Engineer's observations, experience and judgement are correlated and consolidated more effectively by a quantitative system;
- (iii) Engineers prefer numbers in place of descriptions, hence, a quantitative classification system has considerable application in an overall assessment of the rock quality; and
- (iv) Classification approach helps in the organization of knowledge.

While these systems provide valuable tools for engineering design (Bieniawski, 1993), it is important to note that they are not intended as a substitute for detailed engineering procedures, particularly in the final design of complex underground excavations (Bieniawski, 1989)

Rock mass classification systems were first introduced by Ritter (1879) in 1879, when he developed an empirical method for determining the necessary support requirements in tunnels (Evert Hoek, 2007). From that time forward, the systems have evolved into multi-parameter systems, primarily developed through civil engineering projects (Abbas and Konietzky, 2015). The integration of modern support technologies, such as steel ribs, rock bolts, and steel fiber-reinforced shotcrete (SFRS), has further enhanced their applicability (Singh and Goel, 1999).

RMR and Q are among the most widely used classification systems, while GSI is a commonly applied characterization system. Together, these systems play a crucial role in aiding the design of underground structures. These approaches will be further discussed in the following chapter, where their methodologies and applications in engineering design will be explored in more detail. Prior to this, the widely used Rock Quality Designation (RQD) index, a key parameter in both the RMR and Q systems for classifying rock mass quality, will be introduced

3.1.1 Rock Quality Designation

Rock mass designation, RQD, is a well known index for classifying rock mass quality, originally calculated from diamond drill core samples. It was introduced by Don Deer in 1964, and was later incorporated in well known rock mass classification systems like RMR, Q, and the quantified GSI, making it an important parameter in rock mechanics design all over the world. RQD is calculated on cores with a 50 mm diameter as (Pells et al., 2017):

$$RQD = \frac{\sum L_i}{L} \cdot 100 \quad (3.1)$$

where L_i is the length each individual intact core piece that is 100 mm or longer, and L is the total length of the core run. The calculated value is classified into a range that corresponds to descriptive categories, from "excellent" to "worse"; see Table 3.1.1 (Pells et al., 2017).

RQD is a simple and widely used index in classification systems like RMR and Q. However, it has several limitations and challenges. One issue is direction bias in the borehole, which can lead to under-sampling of defects. Additionally, variations in how the system is applied in different parts of

RQD-Based Rock Mass Quality Classification	Range
Excellent	$\geq 90\% - 100\%$
Good	$\geq 75\% - 90\%$
Fair	$\geq 50\% - 75\%$
Poor	$\geq 25\% - 50\%$
Worse	$\leq 25\%$

Table 3.1.1: Rock Quality Designation (RQD) classification and corresponding quality ranges.

the world can result in significantly different RQD values. Misuse of the index includes incorporating fractures that opened after drilling, such as core discing, or including well-defined discontinuities with tensile strength, which were not intended to be part of the calculation Pells et al., 2017.

Another common oversight is ignoring the "hard and sound" criterion originally outlined by Deere. Some practitioners also estimate RQD from rock exposures, deviating from Deere's original method based on core samples. A more detailed discussion of these limitations and their implications can be found in Appendix A, as they will not be elaborated further here. These issues have led some, such as Pells et al. (2017), to recommend phasing out RQD in rock mass classification. The creators of RMR have suggested replacing it with fracture frequency (Pells et al., 2017).

When mapping a tunnel or drift face, various approaches can be used to estimate the RQD. One method involves simply using a measuring rod or tape of one meter in length and counting all rock pieces longer than 10 cm. This method can also be performed using more advanced equipment capable of capturing high-quality face photos or LiDAR scans.

Two other methods involve correlating RQD with other parameters.

$$RQD = 100 e^{0.1\lambda} (0.1\lambda + 1) \quad (3.2)$$

where λ is the average number of discontinuities per meter.

$$RQD = 110 - 2.5 J_v \quad (3.3)$$

where J_v is the volumetric Joint Count, the joints per cubic meter of rock.

3.1.2 Rock Mass Rating

The Rock Mass Rating (RMR) system, introduced by Bieniawski in 1973 (Bieniawski, 1974), is a widely used empirical rock mass classification system for jointed rock masses. RMR₈₉, introduced in 1989, is the most important and commonly used version of the RMR system.

The RMR value can be estimated both from cores and at an excavation face. Ideally, RMR should be determined in the design phase of a project using borehole data and later compared to the RMR estimated during development with data from the face (Celada et al., 2014). When determining RMR, divide the area into structural regions with relatively uniform geological conditions (Bieniawski, 1989), and base the evaluation on typical conditions rather than worst-case scenarios (Palmström, n.d.). It is recommended to assign a range, rather than a single value, to each parameter in order to minimise uncertainties resulting from subjective judgments (Singh and Goel, 1999).

Calculation of the RMR

The following six parameters make up the RMR₈₉ version (Bieniawski, 1989):

R_1 Uniaxial compressive strength of intact rock material (UCS-test or point load index test)

R_2 Rock quality designation (RQD)

R_3 Spacing of discontinuities

R_4 Condition of discontinuities ($JCond_{89}$), given as

$R_{4,1}$ Length, persistence

$R_{4,2}$ Separation

$R_{4,3}$ Smoothness

$R_{4,4}$ Infilling

$R_{4,5}$ Alteration / weathering

R_5 Groundwater conditions (Observed rate of flow into the excavation)

R_6 Orientation of discontinuities

Each parameter designates a value in a given table or graph, based on the condition of the rock. The full table with parameters and ratings is presented in Figure B.0.1. After obtaining all values, RMR is calculated by summarizing these. The RMR system is categorised into various classes, each reflecting the quality of the rock mass. It ranges from very poor rock (0 - 20) to very good rock (81 - 100), and helps engineers assess the stability of rock mass (Bieniawski, 1989).

The RMR system was originally developed using data from civil engineering excavations in sedimentary rocks in South Africa (Bieniawski, 1974). Since more case studies have become available, Bieniawski has published numerous updated versions of the RMR system: 1973, 1974, 1975, 1979, 1989, 2011, 2013 and the most recent one in 2014. The updates include changes in characterization criteria like merging, adding or removing parameters and changing the relative points for each parameter (Rehman et al., 2018).

A major update in 1989 introduced the RMR_{89} , with new graphs and tables for the score of σ_c , RQD, spacing and situation of discontinuities. Within the RMR_{89} system, the basic RMR, RMR_b , can be calculated by summarizing the five first parameters in RMR_{89} , not including *Orientation of discontinuities* (Bieniawski, 1989). This give us the Equation 3.4 and 3.5:

$$\text{RMR}_{89} = R_1 + R_2 + R_3 + R_4 + R_5 + R_6 \quad (3.4)$$

$$\text{RMR}_b = R_1 + R_2 + R_3 + R_4 + R_5 \quad (3.5)$$

An alternative version of the RMR89 system was published in 2013, combining *RQD* (R_2) and *Spacing of discontinuities* (R_3) into a single parameter, joint frequency (R_{2-3}). Joint frequency is the number of discontinuities per meter, and is also a parameter used in RMR14. This modification was introduced to address inconsistencies in the definition and application of RQD across different regions. One major issue was the potential for errors when using rock exposures to determine RQD, leading to inaccurate assessments. The new version aimed to improve the system's overall accuracy (Rehman et al., 2018). This gives us Equation 3.6 and 3.7:

$$\text{RMR}_{89,new} = R_1 + R_{2-3} + R_4 + R_5 + R_6 \quad (3.6)$$

$$\text{RMR}_{b,new} = R_1 + R_{2-3} + R_4 + R_5 \quad (3.7)$$

Using RMR for Support Design

The RMR₈₉ system includes a chart (see Figure 3.1.1) illustrating stand-up time as a function of unsupported span, with RMR values incorporated to allow for estimating rock mass stability. This chart helps engineers predict how long an excavation or tunnel roof can remain stable without support, based on the quality of the rock mass. The figure applies to tunnels with arched roofs, not flat roofs, which have a lower stand-up time. Controlled and precise blasting will further extend stand-up time by minimizing damage to the rock mass (Singh and Goel, 1999).

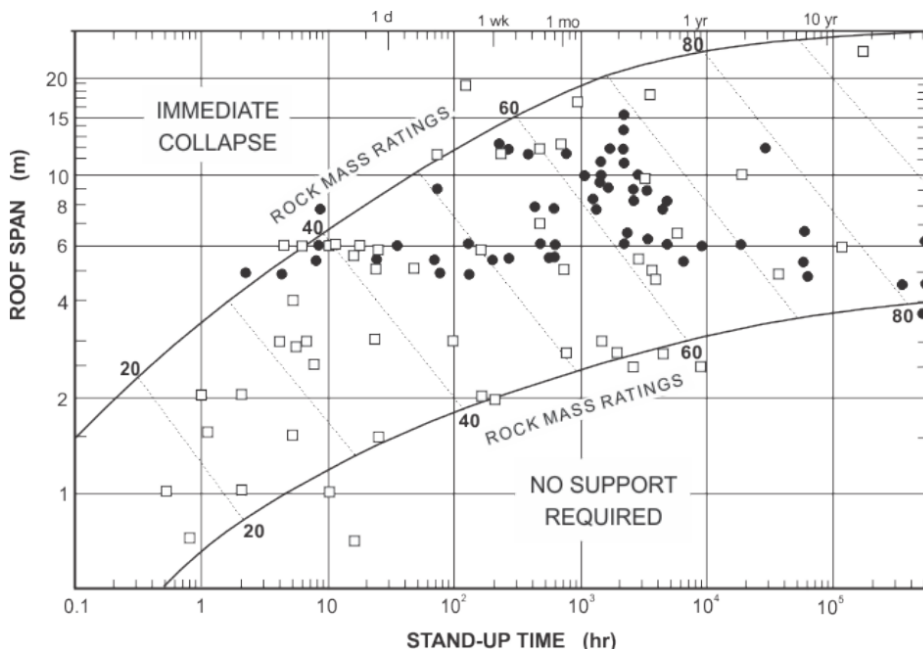


Figure 3.1.1: Stand-up time as a function of unsupported span. RMR values are also given along the contour lines (Bieniawski, 1989).

RMR₈₉ also provides a guide for excavation and support in rock tunnels. The corresponding table provides details on the rock mass class, excavation methods, and support measures such as rock bolts, shotcrete, and steel sets. These recommendations are based on a horseshoe-shaped tunnel with a width of 10 m and a vertical stress, σ_v , of 25 MPa. Details can be found in Table B.0.2.

More in-depth information on the calculation of the updated RMR₁₄, as well as the correlation between RMR₈₉ and RMR₁₄, is presented in Appendix B.

3.1.3 Q-system

The Q-system was developed by NGI in the early 1970's and published in 1974. It was primarily designed for rock mass classification and support design in underground excavations (*Using the Q-system* 2022).

The user-friendly nature of the Q-system has made it accessible to a wide range of professionals. Anyone with a basic understanding of rock mechanics and geology can calculate a Q-value to describe the quality of a rock mass. By incorporating the span or height of the excavation and the type of excavation, the Q-system's rock support chart presented in Figure 3.1.2, provides a recommended support system, specifying the type and quantity of support based on the empirical data. This allows the system to recommend support solutions that have been successfully applied in other projects with comparable Q-values (*Using the Q-system* 2022).

Since its introduction, significant advancements have been made in support philosophy and technologies for underground excavations. These advancements include the introduction of new rock bolts, the development of fiber-reinforced technology, and increasing demands for higher safety factors. As a result, the Q-system has undergone several updates to align with modern support philosophies. Continuous improvements have been made based on new research and practical experiences from tunnel engineering. The support chart was first updated in 1993, based on 1,050 examples primarily from underground excavations in Norway, and then again in 2002, using over 900 additional examples from Norway, India, and Switzerland (*Using the Q-system* 2022).

The Q-value on the support chart ranges from 0.001 to 1,000, with lower values indicating for *exceptionally poor quality squeezing-ground* and higher values indicating *exceptionally good quality rock which is practically unjointed* (Barton et al., 1974). While the Q-system is mainly intended for underground excavations, it can also be applied to field mapping and core logging (Barton et al., 1974). However, these applications may not yield as precise estimates as those obtained directly from underground excavations. This is because the system was developed specifically for underground environments, incorporating parameters like the Stress Reduction Factor (*SRF*) and the Joint Water Reduction Factor (J_w), which can be challenging to accurately estimate from core samples or in field conditions. Moreover, the empirical data used to develop the Q-system comes primarily from tunnels with rock mass influenced by blasting. As a result, Q-values derived from core logging and field map-

ping may be less reliable, and this should be taken into consideration when interpreting the results (*Using the Q-system* 2022).

Most of the data collected during the development of the Q-system comes from projects in hard, jointed rock, often with weakness zones. When working with softer rock that has fewer joints, it is advisable to use other methods together with the Q-system to achieve a more accurate understanding of the rock mass quality. In squeezing or very weak rock, it is recommended to take advantage of deformation measurements and numerical simulations in addition to the Q-system. This combined approach is generally recommended in any case, as it gives a better understanding of the rock mass (*Using the Q-system* 2022).

Calculation of the Q-Value

The Q-value is calculated using the following formula (Barton et al., 1974):

$$Q = \frac{RQD}{J_n} \cdot \frac{J_r}{J_a} \cdot \frac{J_w}{SRF} \quad (3.8)$$

The six key parameters describe various aspects of the rock mass quality and stability (Barton et al., 1974):

- Rock Quality Designation (RQD)
- Joint Set Number (J_n)
- Joint Roughness Number (J_r)
- Joint Alteration Number (J_a)
- Joint Water Reduction Factor (J_w)
- Stress Reduction Factor (SRF)

Each parameter has a defined range and can be determined through field observations, either underground, on the surface, or by core logging. The Q-system provides six descriptive tables, one for each parameter. It is important to note that certain considerations must be taken into account depending on

the methods and conditions under which Q-values are measured or mapped (Barton et al., 1974).

A general recommendation is to calculate multiple Q-values and create a histogram to illustrate the variation in rock mass quality. This becomes especially important with surface mapping, where parameters like J_a and SRF can be challenging to estimate. An estimate of SRF can be based on the overburden, the height of a mountain slope, stress measurements conducted in boreholes, or experiences from nearby construction projects. Because of the challenges of estimating RQD based on surface mapping, the Q-system provides a table for volumetric jointing that can be used as an alternative to RQD (*Using the Q-system* 2022).

The Q-system is built upon three main factors that describe the rock mass stability. These factors are quantified through the parameters used in the calculation of the Q-value, capturing the effects of jointing, friction, and stress on stability (Barton et al., 1974):

$$\frac{\text{RQD}}{J_n} = \text{Degree of jointing (block size)}$$

$$\frac{J_r}{J_a} = \text{Joint friction (inter-block shear strength)}$$

$$\frac{J_w}{\text{SRF}} = \text{Active stress}$$

A smaller block size often correlates with lower stability. However, the rock's hardness also influences how much this factor affects stability. Softer rocks tend to deform more independently of joints compared to harder rocks, and they may absorb stress through internal deformation rather than by fracturing along joints (*Using the Q-system* 2022).

The joint friction factor includes two parameters: joint roughness (J_n) and alteration number (J_a). Like the block size factor, this factor is more important in hard rocks than in soft rocks. In hard rocks, deformation mainly occurs through shear displacement along joint surfaces, while the rock itself stays mostly undeformed. In contrast, deformation in soft rocks is less affected by joints (*Using the Q-system* 2022).

The final factor, active stress, is influenced by the joint water reduction factor (J_w) and the stress reduction factor (SRF). The SRF factor further describes the relationship between the stresses and the strength of the rock mass, which can be observed through signs such as spalling, slabbing, deformation, squeezing, dilatancy, and block release (*Using the Q-system* 2022).

Using the Q-System for Support Design

Once the Q-value is calculated, it serves as a guide for selecting appropriate rock support. Based on documented case histories, the Q-system provides guidelines for support design, tailored to the calculated Q-value and the specific use case. The system is used to evaluate the support on a larger scale than individual blocks, and should therefore never be used to evaluate single blocks or wedges (Barton et al., 1974).

Two essential factors in evaluating support design for underground excavations are safety requirements and excavation dimensions, both depending on the purpose of the opening. Safety requirements are expressed by the excavation support ratio (ESR), while dimensions are defined by the span or height of the excavation (Barton et al., 1974). The ESR value, ranging from 0.5 to approximately 3.5, must be selected from a table and should reflect the purpose of the excavation. A low ESR value, indicating a high safety factor, is suitable for critical projects like nuclear power stations. Higher ESR values represent lower safety factors, appropriate for temporary mine openings (*Using the Q-system* 2022).

These two factors make up the "Equivalent dimension," defined as (Barton et al., 1974):

$$\frac{\text{Span or height in m}}{\text{ESR}} = \text{Equivalent dimension} \quad (3.9)$$

As mentioned in Section 3.1.3, the Q-system provides a rock support chart that suggests a support design (Figure 3.1.2) based on Q-value, ESR, and span or height in meters.

The chart provides detailed information where the Q-value is shown along the bottom horizontal axis, ranging from 0.001 to 1000, and the equivalent dimension is represented on the left vertical axis, ranging from 1 to 100. The top horizontal axis divides rock mass quality into seven main classes, labelled

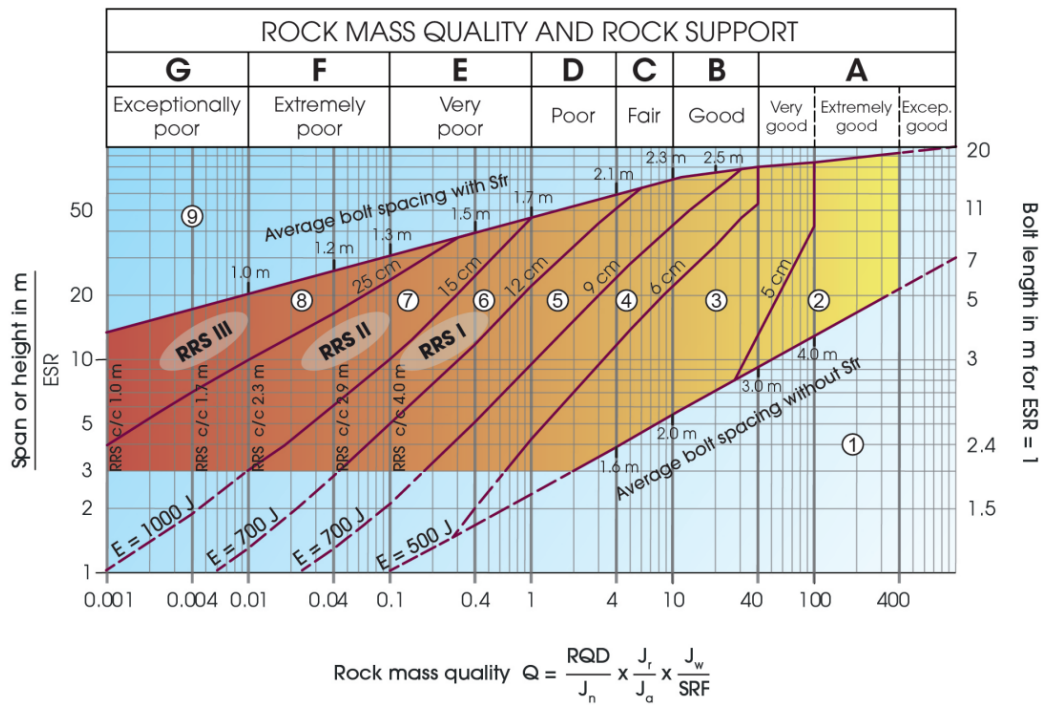


Figure 3.1.2: Rock Support Chart for the Q-system (*Using the Q-system* 2022).

A to G, while the right vertical axis gives additional information about bolt length for ESR = 1.

The chart is further divided into support categories labelled 1 to 9, each with recommended support types. It is important to note that the support recommendations for bolt spacing and sprayed concrete thickness is a continuous scale, even though they are presented as distinct classes. These categories provide guidance on (*Using the Q-system* 2022):

- Rock bolts: Recommended length and spacing
- Fibre reinforced sprayed concrete (RRS): Thickness and energy absorption capacity
- Reinforced ribs of sprayed concrete
- Cast concrete lining

Support recommendations in the chart are general. In particularly challenging cases, increasing the amount or type of support may be necessary (*Using the Q-system* 2022).

The handbook *Using the Q-system*, published by NGI, provides a detailed explanation of the system and guidance on its application in various challenging conditions (*Using the Q-system* 2022). This handbook is regularly updated as new recommendations emerge, so familiarizing oneself with the latest edition is recommended before applying the Q-system to projects.

Modified Q

A modified version of the Q classification system also exists. Q' is a version where SRF and J_w is set to 1. It is used to simplify rock mass classification by focusing solely on properties inherent to the rock mass, excluding the effects of stress and joint orientation, which are accounted for separately in the design process. This avoids double-counting these factors, ensuring a more accurate assessment (Milne et al., 1998). Equation 3.10 is used for calculating Q'.

Q' is particularly useful in mining applications, where environmental and loading conditions are often excluded from the classification. Stress is instead considered in the design steps, such as through the A factor in stability graph methods. Additionally, Q' allows for a clearer evaluation of rock masses in conditions where shear or fault zones exist, as these are considered part of the rock mass rather than stress-related factors (Milne et al., 1998).

$$Q' = \frac{\text{RQD}}{J_n} \times \frac{J_r}{J_a} \quad (3.10)$$

The Q' value can be applied both during core-logging and as a parameter in a formula for stope dimensioning, where it helps determine appropriate excavation dimensions (Milne et al., 1998).

3.1.4 Geological Strength Index

Building on the overview presented in Section 2.5.2, this section provides a more detailed exploration of the Geological Strength Index (GSI) system. It is recommended to read Section 2.5.2 in advance, for a detailed understanding of how GSI integrates into the generalised Hoek-Brown failure criterion.

The Geological Strength Index (GSI) is a widely used characterization system for assessing rock mass strength properties. Developed by Hoek and Marinos in 1994, GSI was designed to provide reliable input data for the generalised Hoek-Brown failure criterion and is primarily used to derive key rock mass parameters required for analytical and numerical methods. These include rock mass material constants m_b , s and a , as well as the deformation modulus E_m , rock mass strength σ_{cm} , cohesion c_m , and friction angle ϕ_m . By reducing σ_{ci} and m_i obtained from laboratory tests or indexes, GSI ensures these parameters align more with the in-situ conditions. A spreadsheet for calculating the rock mass properties based on σ_{ci} , m_i and GSI is presented by P. Marinos and Evert Hoek (n.d.).

Unlike classification systems focused on support design, GSI emphasizes direct geological observations in the field, capturing key properties such as rock mass structure and surface conditions through visual assessments. This qualitative approach allows engineers to make informed estimates of rock mass properties in cases where quantitative systems may fall short, especially in very weak or tectonically disturbed rock masses (E. Hoek and Brown, 2019).

As mentioned in 2.5.2; GSI can only be used on homogeneous and isotropic rock mass. This assumption applies to heavily jointed rock masses where failure occurs primarily through sliding along discontinuities or rotation of blocks. In such cases, there is little or no failure of the intact rock pieces, and no preferred failure directions (E. Hoek and Brown, 2019).

The GSI was initially developed as a tool for the preliminary estimation of rock mass properties, with the understanding that these estimates would be refined through detailed site investigations, numerical analyses, and back analyses for validation and calibration (E. Hoek and Brown, 2019).

Determining the GSI Range

The GSI system provides a chart, presented in Figure 3.1.3, that combines both visual and descriptive elements to guide the user choosing the correct GSI values. It consists of two main parameters, that primarily influences the mechanical properties of a rock mass. The *structure* on the y-axis, describes blockiness, while the y-axis describes *surface quality*. GSI values range from 0 to 100, where higher GSI values indicate better quality rock mass (E. Hoek and Brown, 2019).

The GSI values, like intact rock properties, should not be treated as single fixed numbers but rather as distributions that reflect the inherent variability of rock masses. Determining GSI involves focusing on the shape of the blocks and the characteristics of the discontinuities that separate them, rather than on block size. Since assigning a precise numerical value to GSI is impractical for most rock masses, it is best represented as a range of values. For analytical purposes, this range can be modelled using a normal distribution characterised by a mean and standard deviation, capturing the natural uncertainty and variability inherent in geological conditions (V. Marinos et al., 2005).

As a visual system, GSI can be subjective and may lead to variability between users. This emphasizes the importance of assigning a range of values rather than relying on a single fixed value.

P. Marinos and Evert Hoek (n.d.) also presents typical GSI ranges for various rock types, including sandstone, siltstone, claystone, clay shale, limestone, granite, ophiolites, gneiss, schist, and heterogeneous rock masses such as flysch. These ranges are designed to assist with field mapping, offering a practical tool for geologists and engineers. While deviations may occur, they are generally exceptions, ensuring the charts provide reliable guidance for most cases.

Several authors have proposed quantified versions of the qualitative GSI system, making it more accessible for inexperienced geologists and engineers who may lack a strong understanding of rock mass variability. Evert Hoek, Carter, et al. (2024) introduced a GSI chart based on Joint Condition ($JCond_{89}$) and RQD, two parameters introduced in subsections 3.1.2 and 3.1.1, respectively. The quantified GSI chart is presented in Figure 3.1.4.

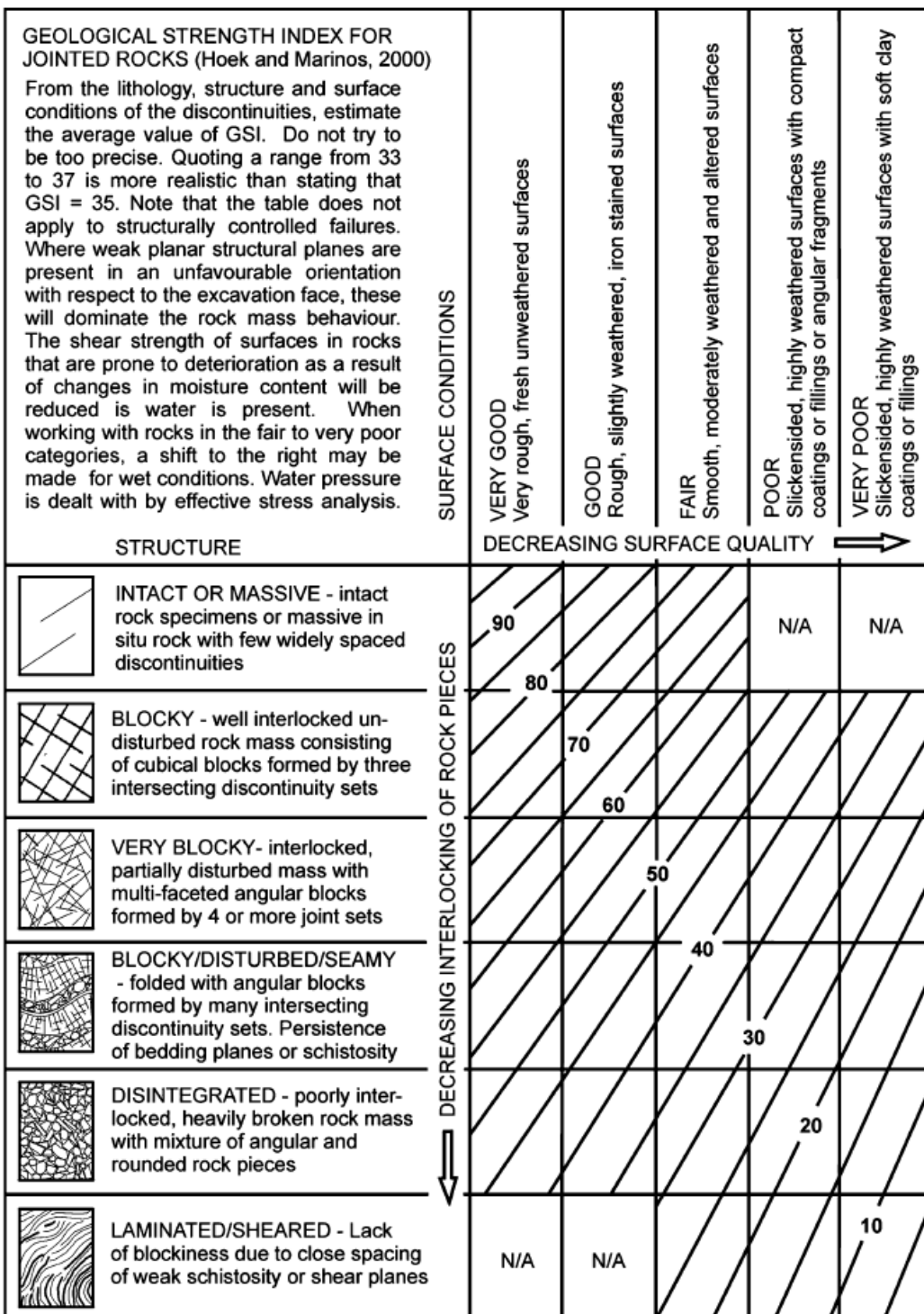


Figure 3.1.3: Basic chart for GSI, based on geological observations (E. Hoek and Brown, 2019).

The quantified GSI is expressed as:

$$GSI = 1.5 \cdot JCond_{89} + \frac{RQD}{2} \quad (3.11)$$

Another version, also presented by Evert Hoek, Carter, et al. (2024), can be applied when $JCond_{89}$ is not available. This approach uses Jr and Ja from the Q-system, allowing the quantified GSI to be calculated as:

$$GSI = \frac{52 Jr/Ja}{1 + Jr/Ja} + \frac{RQD}{2} \quad (3.12)$$

With GSI (qualitative or quantitative), σ_{ci} , m_i , and D , one can obtain the complete set of strength and deformability parameters of the rock mass, making GSI a crucial tool for estimating rock mass behaviour in engineering support design and analysis (E. Hoek and Brown, 2019).

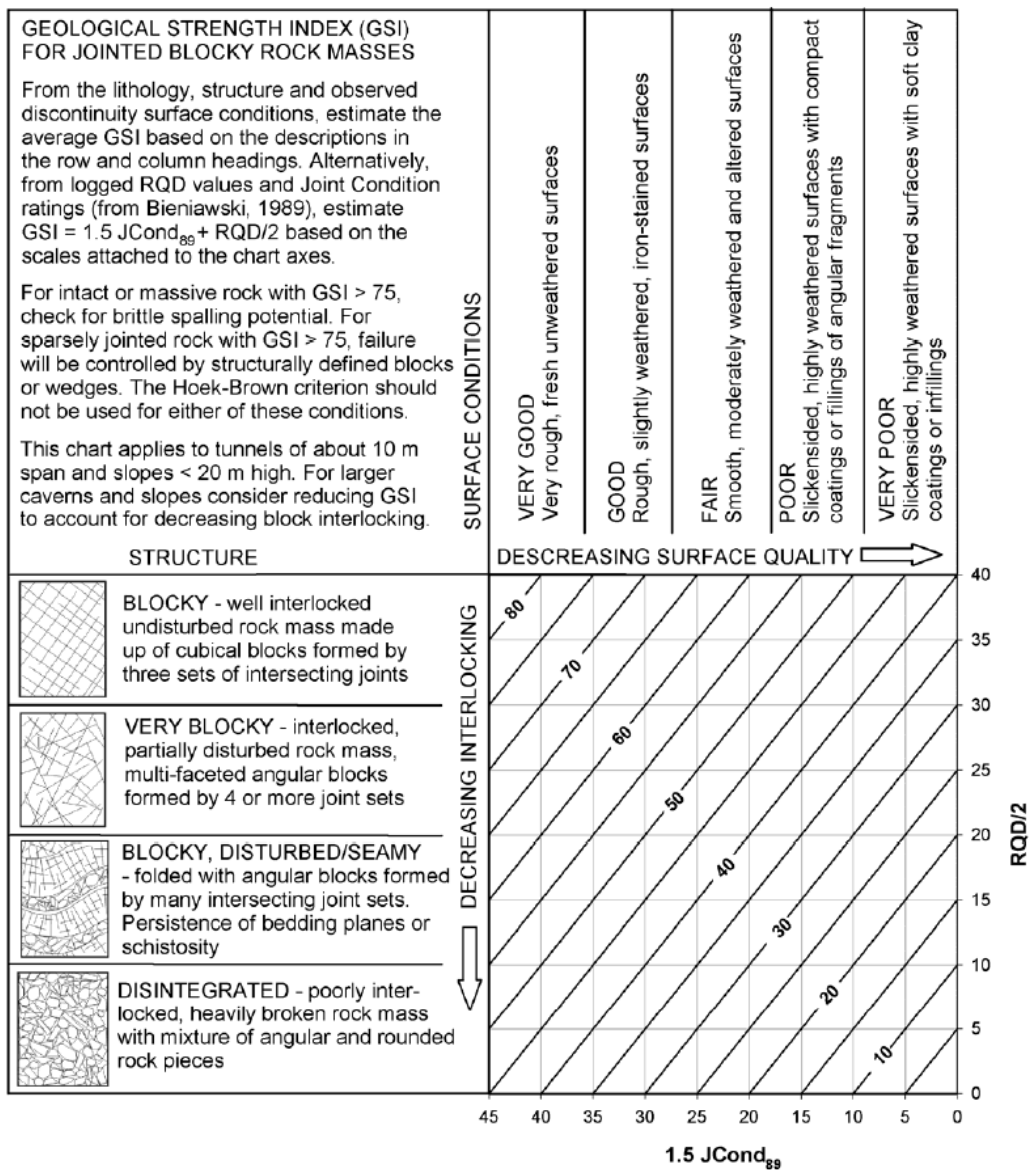


Figure 3.1.4: Quantification of GSI by Joint Condition and RQD (Evert Hoek, Carter, et al., 2024).

3.1.5 Calculation of Rock Mass Design Parameters Using Rock Mass Classification and Characterization Systems

The purpose of this subsection is to present empirical equations for estimating the rock mass design parameters introduced in Section 2.1.3. The parameters covered include the deformation modulus (E_m), rock mass strength (σ_{cm}), tensile strength of the rock mass (σ_{tm}), Poisson's ratio of the rock mass (ν_m), shear modulus of rock mass G_m , as well as the Mohr-Coulomb parameters cohesion (c_m) and friction angle (ϕ_m), both for the rock mass.

Many empirical equations have been proposed for estimating the deformation modulus. L. Zhang (2017) provides a comprehensive review of various empirical methods, some of which are presented in Table 3.1.2.

Additionally, Vásárhelyi and Kovács (2017) presents empirical equations for estimating rock mass strength, tensile strength of the rock mass, Poisson's ratio, cohesion, and friction angle for rock masses. Selected equations from this study are summarised in Tables 3.1.3, 3.1.4, 3.1.5, and 3.1.6. The last empirical equation in Table 3.1.3 for estimating σ_{cm} was suggested by (P. Marinos and Evert Hoek, n.d.).

Some of the presented equations require the Hoek-Brown parameters s and a . These parameters can be determined using Equations 2.26 and 2.27.

Some equations also use the factor f_c . It is defined as $\frac{\sigma_c}{100}$ for $Q > 10$, and otherwise, it equals 1. Additionally, γ represents the unit weight of the rock mass in [g/cm^3].

Carranza-Torres and Fairhurst (2000) presents the estimation of the shear modulus which will be presented after the tables.

Table 3.1.2: Empirical equations for calculating E_m

Equation (GPa)	Parameter(s)
$E_m = E_i \cdot 10^{0.0186 \cdot \text{RQD} - 1.91}$	RQD, E_i
$E_m = 0.1 \cdot \left(\frac{\text{RMR}}{10}\right)^3$	RMR
$E_m = 0.0736 \cdot e^{0.0755 \cdot \text{RMR}}$	RMR
$E_m = E_i \cdot 10^{[(\text{RMR} - 100) \cdot ((100 - \text{RMR})/4000) \cdot \exp(-\text{RMR}/100)]}$	RMR, E_i
$E_m = 25 \cdot \log Q$	Q
$E_m = 10 \cdot \left(Q \cdot \frac{\sigma_c}{100}\right)^{1/3}$	Q, σ_c
$E_m = 0.1451 \cdot e^{0.0654 \cdot \text{GSI}}$	GSI
$E_m = \tan(\ln(\text{GSI})) \cdot \log(\sigma_c) \cdot (\text{RQD})^{1/3}$	GSI, RQD, σ_c
$E_m = \tan\left(\sqrt{1.56 + (\ln(\text{GSI}))^2}\right) \cdot (\sigma_c)^{1/3}$	GSI, σ_c
$E_m = E_i \cdot \left(0.02 + \frac{1 - \frac{D}{2}}{1 + \exp\left(\frac{60 + 15 \cdot D - \text{GSI}}{11}\right)}\right)$	GSI, E_i, D

Table 3.1.3: Empirical equations for calculating σ_{cm}

Equation (MPa)	Parameter(s)
$\frac{\sigma_{cm}}{\sigma_c} = -0.0157 \cdot \text{RQD} - 0.7667 \quad (70 \leq \text{RQD} \leq 100)$	RQD
$\frac{\sigma_{cm}}{\sigma_c} = 0.0231 \cdot \text{RQD} - 1.32 \geq 0.15$	RQD
$\frac{\sigma_{cm}}{\sigma_c} = 10^{0.0012 \cdot \text{RQD} - 1.34}$	RQD
$\sigma_{cm} = 0.5 \cdot e^{0.06 \cdot \text{RMR}}$	RMR
$\frac{\sigma_{cm}}{\sigma_c} = e^{\frac{\text{RMR}-100}{20}}$	RMR
$\frac{\sigma_{cm}}{\sigma_c} = e^{\frac{\text{GSI}-100}{18.5}}$	GSI
$\sigma_{cm} = 7 \gamma f_c Q^{1/3} \quad (\text{MPa})$	Q, f_c , γ
$\sigma_{cm} = \sqrt{s \cdot \sigma_c}$	HB constant s , σ_c
$\sigma_{cm} = s^a \cdot \sigma_c$	2002 HB constant s and a , σ_c
$\sigma_{cm} = (0.0034 m_i^{0.8}) \sigma_{ci} \{1.029 + 0.025e^{-0.1m_i}\}^{\text{GSI}}$	GSI, m_i , σ_{ci}

Table 3.1.4: Empirical equations for calculating σ_{tm}

Equation (MPa)	Parameter(s)
$\sigma_{tm} = -\frac{s \sigma_{ci}}{m_b}$	σ_{ci}, m_b , HB constant s
$\sigma_{tm} = 0.5 \sigma_c \left[m_b - (m_b^2 + 4s)^{0.5} \right]$	σ_c, m_b , HB constant s
$\frac{\sigma_{tm}}{\sigma_t} = \frac{\text{RMR}}{\text{RMR} + 6(100 - \text{RMR})}$	RMR, σ_t
$\sigma_{tm} = -0.029 \gamma f_c Q^{1/3} \quad (\text{MPa})$	Q, f_c , γ

Table 3.1.5: Empirical equations for calculating ν_m

Equation	Parameter(s)
$\nu_m = 0.25 \left(1 + e^{-\sigma_{cm}/4}\right)$	σ_{cm}
$\frac{\nu_m}{\nu_i} = 2.5 - 1.5 \cdot \frac{\text{RMR}}{\text{RMR} + (100 - \text{RMR})}$	RMR, ν_i
$\nu_m = -0.002 \cdot \text{GSI} + \nu_i + 0.2$	GSI, ν_i
$\nu_m = -0.002 \cdot \text{GSI} - 0.003 \cdot m_i + 0.457$	GSI, m_i

Table 3.1.6: Empirical equations for calculating c_m and ϕ_m

Equation	Parameter(s)
$c_m = 3.625 \text{ RMR}$	RMR
$\phi_m = 25 [1 + 0.01 \text{ RMR}] \quad \text{for RMR} \geq 20\%$	RMR
$\phi_m = 1.5 \text{ RMR} \quad \text{for RMR} < 20\%$	RMR
$\phi_m = 20 \cdot \sigma_{cm}^{0.25}$	σ_{cm}
$\phi_m = 20 + 0.5 \text{ RMR}$	RMR
$c_m = \frac{\sigma_{cm}}{2} \frac{1 - \sin \phi_m}{\cos \phi_m}$	σ_{cm}, ϕ_m
$c_m = \frac{\text{RMR}}{\text{RMR} + 6(100 - \text{RMR})} c_i$	RMR, c_i
$c_m = \left(\frac{\text{RQD}}{J_a} \cdot \frac{1}{\text{SRF}} \cdot \frac{\sigma_c}{100} \right)$	RQD, SRF, σ_c, J_a
GSI	s, mb

The rock mass shear modulus can be calculated using the classic relationship from isotropic elasticity (Carranza-Torres and Fairhurst, 2000):

$$G_m = \frac{E_m}{2(1 + \nu_m)}$$

3.1.6 Comparison of Empirical Methods

The RMR, Q, and GSI are commonly used empirical methods for classifying and characterising rock masses and designing rock support in underground excavations. Although these systems share some similarities, they differ significantly in their structure, input parameters, and application. These differences are outlined below (Palmström, 2008).

The calculation methodologies for the three systems differ significantly. RMR is calculated by summing the ratings of specific parameters while the Q-system combines input parameters through multiplication and division. GSI qualitatively assesses rock properties through observations but can also be calculated by direct numerical parameters with the quantified version (Palmström, 2008).

These three methods also vary in how they guide support design. RMR provides support recommendations through tables developed for 10-meter wide tunnels, while the Q-system uses charts that relate the Q-value with tunnel dimensions. GSI does not directly propose support measures but is used as an input for both analytical models and numerical models Palmström (2008).

The treatment of rock properties and stress conditions highlights further differences. RMR, unlike Q, explicitly includes parameters like UCS but does not account for how in situ stresses and stress-related conditions impact rock mass stability, like the Q-system does with its SRF parameter (Palmström, 2008) .

The consideration of rock properties and stress conditions also varies. RMR explicitly includes parameters such as U, unlike the Q-system. However, the Q-system incorporates in situ stress effects through SRF, which allows it to address stress-related instability, a limitation of RMR. GSI does not account for stress conditions directly, instead relying on external analyses for such considerations (Palmström, 2008).

RMR and Q may be less relevant in conditions with large water inflows, as the application of shotcrete is challenging in such environments (Palmström, 2008). Both systems, however, account for water conditions to some extent. RMR includes groundwater as an explicit parameter, and the Q-system considers it through the Jw factor. GSI does not directly address water conditions but recommends shifting the GSI value to the right for "fair to very

poor" discontinuities in wet conditions (V. Marinos et al., 2005).

Weakness zones present a notable challenge in rock mass classification. The Q-system partially incorporates these zones through the SRF parameter, while RMR lacks a dedicated parameter for this. According to Palmström (2008), the complexity of weakness zones makes them difficult to address adequately in any classification system, and both RMR and Q have significant limitations in this regard. GSI, in contrast, evaluates weakness zones qualitatively based on their structure and thickness, offering flexibility but sacrificing precision. None of these systems fully address extreme ground conditions such as squeezing, swelling, or ravelling, which require additional tools and methods for proper evaluation and support design (Palmström, 2008).

RMR performs well in competent rock masses but tends to be unreliable in weak or highly fractured conditions, partially because of RQD. Similarly, the Q-system can face limitations in weak ground, which may be difficult to quantify accurately in highly fractured or altered zones. GSI, on the other hand, is better suited for characterising weak or fractured rock masses (Palmström, 2008).

Applying rock mass classification systems in support design requires considerable engineering judgment. These systems are useful as guidelines, but final decisions on rock support should always consider site-specific conditions and be guided by experienced engineers (Palmström, 2008). Because of these limitations, these empirical systems should be used together and compared to ensure a more comprehensive understanding of the rock mass and to validate support recommendations by each system.

Each classification system uses different parameters, making direct conversion between them unreliable and not advisable. While correlations can be helpful for preliminary assessments when specific data is unavailable, they introduce inaccuracies due to differences in how parameters are evaluated. As such, correlations should be used with caution and supplemented by engineering judgment (Abbas and Konietzky, 2015).

Some empirical relationships between *RMR* and *GSI* as discussed by Q. Zhang et al. (2019) are presented below.

$$\begin{aligned}
 \text{RMR}_{89} &= \text{GSI} + 5 \\
 \text{RMR}_{89} &= 2.38 \text{ GSI} - 54.93 \\
 \text{RMR}_{89} &= 20 \ln \left(\frac{\text{GSI}}{6} \right) \\
 \text{RMR}_{89} &= 1.35 \text{ GSI} - 16.40 \\
 \text{RMR}_{89} &= 1.36 \text{ GSI} + 5.90 \\
 \text{RMR}_{89} &= 1.01 \text{ GSI} + 4.95
 \end{aligned}$$

Milne et al. (1998) compiled several empirical equations relating *RMR* and *Q*. These equations are listed below.

$$\begin{aligned}
 \text{RMR} &= 13.5 \log Q + 43 \\
 \text{RMR} &= 9 \ln Q + 44 \\
 \text{RMR} &= 12.5 \log Q + 55.2 \\
 \text{RMR} &= 5 \ln Q + 60.8 \\
 \text{RMR} &= 43.89 - 9.19 \ln Q \\
 \text{RMR} &= 10.5 \ln Q + 41.8 \\
 \text{RMR} &= 12.11 \log Q + 50.81 \\
 \text{RMR} &= 8.7 \ln Q + 38 \\
 \text{RMR} &= 10 \ln Q + 39
 \end{aligned}$$

Singh and Goel (1999) presents a correlation between GSI and *Q'* for poor rock quality rock masses:

$$\text{GSI} = 9 \ln Q' + 44$$

3.1.7 Applications and Limitations

Empirical methods are widely used in rock mass classification and support design because they provide quick and straightforward estimates of rock mass quality and parameters. They are particularly effective in the early stages of design and for tunnels or drifts but can also be used throughout an entire project. The different systems have distinct strengths and weaknesses, making it important to combine and compare them with one another (Abbas and Konietzky, 2015).

However, these methods have notable limitations. They fail to account for complex stress redistribution, time-dependent behaviours like creep, and detailed geometrical factors such as shear zones or other complex geometries. Systems like RMR and Q may provide support recommendations but do not consider interactions between support elements or accurately address extreme conditions. GSI, while flexible, is prone to subjectivity, making its reliability dependent on the user's expertise. As such, empirical methods should be supplemented with engineering judgment and additional analytical and numerical tools for more optimized design solutions (Abbas and Konietzky, 2015).

3.2 Analytical Design Methods

Analytical methods are structured approaches that use mathematical formulations to predict the behaviour of rock masses and support systems in underground excavations. Compared to empirical methods, which rely on observed data and generalised relationships, analytical methods provide a deeper understanding of the deformation mechanisms and the interaction between the rock mass and the applied support. This makes them valuable for understanding specific designs under varying conditions, providing more detailed analysis than empirical methods for tunnel stability and support design (Paraskevopoulou and Diederichs, 2018).

3.2.1 Convergence-Confinement Method

The Convergence-Confinement Method (CCM) is a widely recognised empirical approach for designing support systems in underground excavations. It

utilizes three main components: the Ground Reaction Curve (GRC), Support Reaction Curve (SRC), and Longitudinal Displacement Profile (LDP) (Paraskevopoulou and Diederichs, 2018). Figure 3.2.2 provides an overview of these terms.

Using the GRC and SRC, it is possible to analyze displacement and stress around a circular opening under a 2D hydrostatic stress field. The LDP adjusts and interprets the relationship between support pressure, radial displacement, and distance from the excavation face. Together, the GRC, SRC, and LDP provide a simplified yet effective understanding of rock mass and support interactions, serving as valuable tools in assessing support requirements (Carranza-Torres and Fairhurst, 2000).

The GRC represents the relationship between the radial displacement of a tunnel wall and the support pressure needed to maintain stability. Radial displacement is the inward or outward movement of the rock surface, while support pressure is the outward force exerted by the support system. The radius of the circular opening, hydrostatic stress, and uniform support pressure are denoted by r_0 , p_0 , and p_i , respectively, as shown in Figure 3.2.1. The distance from the opening center to the plastic zone edge is labeled r_p (Carranza-Torres and Fairhurst, 2000).

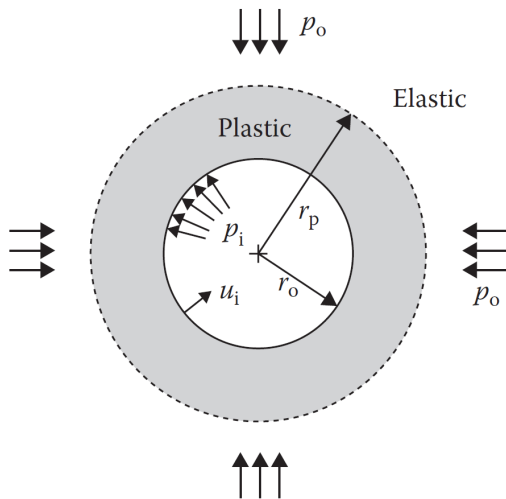


Figure 3.2.1: Circular opening under hydrostatic stress field p_0 and uniform support pressure p_i , illustrating zones of elastic and plastic deformation (Karpuz and Basarir, 2015).

The top left corner of Figure 3.2.2 illustrates the LDP. As shown, deformation begins before the excavation face and is zero when p_i equals p_0 . Moving away from the face, deformation increases as p_i falls below p_0 , reaching maximum deformation u_{rm} when p_i equals zero, assuming no support measures are in place. L_0 represents the distance behind the face where support is added, resulting in deformation u_{s0} (Carranza-Torres and Fairhurst, 2000). The dotted line traces down to the GRC in the figure's bottom right corner.

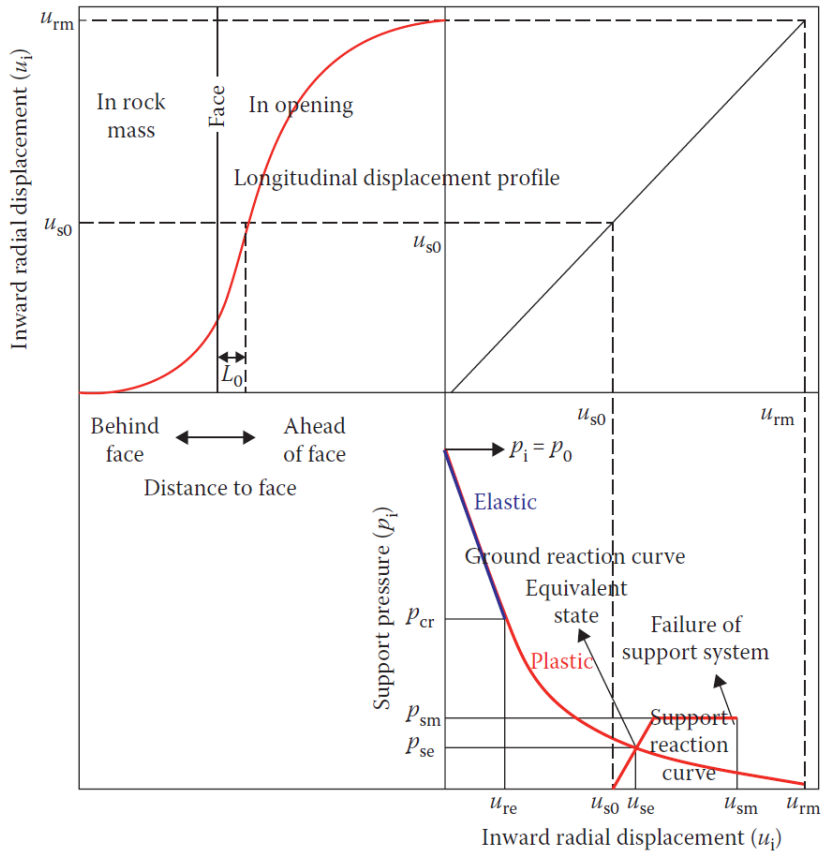


Figure 3.2.2: Interaction between LDP, GRC, and SRC, showing the relationship between support pressure, radial displacement, and distance from the excavation face (Karpuz and Basarir, 2015).

The GRC can be divided into two sections: an elastic section (blue line) and a plastic section (red line), divided by the critical support pressure, p_{cr} (Carranza-Torres and Fairhurst, 2000). The elastic part is linear, indicating elastic deformation, while the plastic part is nonlinear, representing plastic deformation.

Once a support system is installed, its action is activated by rock deformation. Support pressure increases with deformation, as shown by the SRC (red) in Figure 3.2.2. When the SRC intersects the GRC at support pressure p_{se} , deformation ceases at rock displacement u_{se} . The maximum support pressure produced by the system is p_{sm} , beyond which failure occurs at deformation u_{sm} (Carranza-Torres and Fairhurst, 2000).

Achieving low deformation requires a support system capable of higher support pressure, typically installed earlier, but at greater cost. Delaying support installation allows for more deformation but reduces support pressure requirements. Therefore, the timing of support installation depends on acceptable deformation limits and system cost (Carranza-Torres and Fairhurst, 2000).

Several methods exist to construct the GRC, including those by Duncan Fama (1993) and Carranza-Torres and Fairhurst (2000). The primary difference lies in the chosen rock mass failure criterion and whether the rock mass dilates during failure (Kargar, 2019).

Duncan Fama's method employs the Mohr-Coulomb criterion, assuming no dilation, which is suitable for cases with minimal rock dilation (Kargar, 2019). Carranza-Torres and Fairhurst's method uses the generalised Hoek-Brown criterion and includes dilation, making it applicable for situations with post-failure rock expansion (Carranza-Torres and Fairhurst, 2000).

To construct the SRC, the elastic stiffness K_s and maximum support pressure p_{sm} must be calculated for each support device. Carranza-Torres and Fairhurst (2000) provided formulas for shotcrete, blocked steel sets, and ungrouted bolts and cables. When analyzing a support system with multiple devices, their elastic stiffness values can be combined to increase the support system's slope. The system fails when one device reaches its maximum elastic deformation u_{sm} (Carranza-Torres and Fairhurst, 2000).

3.2.2 Applications and Limitations

Analytical methods, particularly the Convergence-Confinement Method (CCM), are valuable tools in support design as they provide a description of the rock-support interaction. CCM is particularly useful in preliminary design phases, offering rapid estimates of deformation, plastic zones, and required support loads. Additionally, the method is efficient for estimating convergence and

plastic zone extents in tunnels, even when non-circular openings are approximated with an equivalent radius. These advantages make CCM an essential addition to the design process. However, the method has limitations worthy of note (Carranza-Torres and Fairhurst, 2000).

The method assumes a 2D idealised geometry (circular opening), hydrostatic stress fields, uniform support pressure, and homogeneous, isotropic rock. These simplifications can lead to inaccuracies in more complex scenarios. Time-dependent behaviours, such as creep or rheological effects, are not explicitly considered, which can affect the predictions of deformation and support loads. Furthermore, for tunnels with high horizontal-to-vertical stress ratios or irregular geometries, CCM's accuracy diminishes, and numerical modelling becomes necessary to capture the complexities of the rock mass and ensure reliable design outcomes (Carranza-Torres and Fairhurst, 2000).

3.3 Numerical Modelling Approaches

Numerical modelling is a widely adopted approach in rock mechanics, used to simulate and predict the behaviour of rock materials under various conditions. Rock is a complex, naturally occurring material with varying minerals, discontinuities, and weaknesses, making its behaviour challenging to predict (Nikolić et al., 2016). Despite these complexities, numerical models help estimate stresses and deformations in both 2D and 3D, providing valuable insights into engineering problems that cannot be fully addressed using empirical or analytical methods (Lorig et al., 2013).

Numerical methods originated in the 1960s, and with the rapid advancement of computers and increased computational power since then, these methods have evolved to solve increasingly complex problems. They allow for flexible geometries and more accurate predictions of rock mass behaviour, accounting for factors such as anisotropy, inhomogeneity, pre-existing stress states, and time-dependent behaviours like creep and plastic deformation (Nikolić et al., 2016).

Numerical models in rock mass are usually implemented in either two or three dimensions, depending on the geometric characteristics of the problem and the desired level of detail (Nikolić et al., 2016). 2D models are often used for analyzing stresses and displacements in cases where one dimension

can be assumed to be uniform, such as in a long tunnel where the cross-sectional geometry is consistent. This approach is computationally efficient and suitable for plane strain analyses, where one of the displacement components remains constant. 3D modelling is necessary when end effects or variations along all dimensions cannot be neglected, such as in irregularly shaped or short drifts. While 3D models offer a higher level of accuracy, they require significantly more computational power and time, often necessitating additional assumptions to simplify the problem (Jing and Hudson, 2002).

Back-analysis is a critical step in the numerical modelling process. By using field measurements, such as displacements or tunnel convergence, back-analysis refines the model to better match site-specific conditions. This iterative process continuously updates the model as the rock mass changes, improving its accuracy and reliability throughout the project. Incorporating large-scale field data also naturally accounts for scale effects, making back-analysis an essential tool for calibrating material properties and validating numerical simulations (Jing and Hudson, 2002).

Numerical methods can be divided into three main categories: continuum, discontinuum, and hybrid continuum/discontinuum methods. This chapter introduces continuum and discontinuum methods and presents popular sub-approaches within each branch. The hybrid methods combine elements of both approaches (Nikolić et al., 2016), however they are beyond the scope of this discussion.

The choice of modelling approach depends largely on the specific problem to be solved, with particular emphasis on the scale of the problem and the geometry of the fracture system (Nikolić et al., 2016).

3.3.1 Continuum Methods

Continuum methods treat the rock mass as a continuous medium, making them suitable for large-scale problems where discontinuities play a less significant role. These methods can still accommodate the presence of a limited number of joints, as long as the fractures do not result in significant block detachment or opening. In such cases, the spacing between joints must be sufficiently large relative to the scale of the engineering problem, ensuring that individual blocks remain stable and do not detach or move independently (Jing and Hudson, 2002).

Some popular continuum methods are Finite Differential Method (FDM), Finite Element Method (FEM) and Boundary Element Method (BEM). BEM is a integral method, using approximations on the boundary of the opening, while FDM and FEM is a differential method, using approximations throughout the entire problem domain (Jing and Hudson, 2002). RS2 is an example of software that utilizes the Finite Element Method (*RS2 / 2D Geotechnical Finite Element Analysis / Rocscience 2024*). FEM and RS2 will be introduced further in the next subsection.

Finite Element Method and RS2

The Finite Element Method (FEM) is one of the most widely used numerical methods for advanced simulations in soil and rock mechanics, particularly for capturing nonlinear, time-dependent, and anisotropic behaviours. Originally developed as an alternative to the Finite Difference Method (FDM), FEM emerged as the superior approach during the 1960s and 1970s. Its success was largely due to its ability to effectively handle material heterogeneity, nonlinear deformability (plasticity), complex boundary conditions, in-situ stresses, and gravity (Nikolić et al., 2016).

FEM works by dividing a complex problem domain into smaller, simpler parts called finite elements, which together form a mesh. Each element is connected at discrete points called nodes. Within each element, the unknown quantity, such as displacement or stress, is approximated using mathematical functions, based on nodal values. These local approximations are assembled into a global matrix that represents the entire system. Once the finite element assembly is complete, the algebraic system of equations is solved to determine the nodal values, which are used to calculate quantities of interest throughout the domain (Nikolić et al., 2016).

Several advanced FEM methods have been developed to address specific challenges in rock mechanics. Extended FEM (X-FEM), Embedded Discontinuity FEM (ED-FEM), and Generalised FEM (G-FEM) are notable examples. These methods expand the applicability of FEM to include fracture growth, large displacements, and other discontinuous behaviours, making them highly effective in scenarios involving joints and fractures. These methods will not be explained further (Nikolić et al., 2016).

Traditional FEM faces challenges in accurately modelling joints and discontinuities because it is based on continuum assumptions. Joint elements were

introduced to approximate the behaviour of discontinuities. These elements simulate small displacements across fractures but cannot model large-scale movements, such as sliding or complete detachment. Enhanced FEM methods, such as X-FEM and ED-FEM, can overcome these limitations by incorporating discontinuous functions and enabling the representation of large-scale fracture propagation and non-linear behaviours (Nikolić et al., 2016).

FEM offers significant flexibility due to its ability to model heterogeneous materials by dividing the domain into different elements, each with its own material properties. Another advantage is the use of unstructured and irregular meshes, which enables FEM to handle complex geometries more effectively and adapt to localised phenomena. In areas with high stress, large deformations, or material transitions, irregular meshes provide higher resolution and more accurate calculations where needed, without adding unnecessary complexity to the entire model (Nikolić et al., 2016).

Furthermore, FEM is well-suited for representing non-linear and inelastic behaviours, such as material hardening, softening, and plasticity. This flexibility, combined with its ability to capture interactions across different scales, from nano- to macro-level phenomena, makes FEM an essential tool for solving complex engineering problems in rock mechanics (Nikolić et al., 2016).

While FEM offers numerous advantages, it also has some limitations. Although FEM is capable of estimating behaviours across different scales, it is most effective for problems involving significant deformations or complex material behaviours and may be less efficient for small-strain problems, where simpler methods can be more accurate. Additionally, FEM can be computationally intensive, as solving the global system of equations and handling complex meshes requires significant time and resources, particularly for large-scale or highly detailed models. This is especially true for large 3D simulations (Nikolić et al., 2016).

One of the most prominent commercial FEM software tools for geotechnical applications, including rock mechanics, is PLAXIS (Nikolić et al., 2016). Similarly, RS2 is another widely used FEM-based software designed specifically for geotechnical and rock engineering analyses (*RS2 / 2D Geotechnical Finite Element Analysis / Rocscience* 2024).

RS2 is a "Rock and Soil 2-Dimensional Analysis Program" which uses FEM for applications in tunnel and support design, underground excavation, and other rock engineering analyses (*RS2 / 2D Geotechnical Finite Element Anal-*

ysis / Rocscience 2024). A 3D version called RS3 also exists (RS3 / 3D Finite Element Software For Advanced Analysis / Rocscience 2024). However, it will not be discussed further.

RS2 enables users to simulate stress, deformation, and failure in rock masses through advanced modelling capabilities. By dividing the domain into finite elements, the software can handle complex geometries, heterogeneous materials, and behaviours ranging from elastic (linear) to plastic (non-linear). Key features include the ability to model multiple stress fields, groundwater flow, and staged excavation with support installation. The software also supports probabilistic analysis, such as Monte Carlo simulations, to assess variability in material and joint properties. Visual outputs, including stress, displacement, and yielded elements, allow engineers to evaluate stability and design performance under various conditions (RS2 / 2D Geotechnical Finite Element Analysis / Rocscience 2024).

Figure 3.3.1 shows an example of a plastic model in heavily jointed rock presented in the "RS2 User Guide." The model is analysed with various forms of support. The coloured contours visualise the strength factor, which is the ratio of a material's strength to the applied stress. The red arrows represent displacement (RS2 Tutorials / Adding Support 2024).

The model on the left has no support, the one in the middle uses bolts, and the one on the right includes both bolts and shotcrete (RS2 Tutorials / Adding Support 2024). As expected, more support and higher internal pressure result in less deformation.

3.3.2 Discontinuum Methods

Discontinuum methods are most suitable for rock masses with a moderate to high density of fractures, where the number and behaviour of fractures exceed the capacity of continuum methods or where large-scale displacements of individual blocks are expected. These methods explicitly consider the presence of fractures, joints, and other discontinuities, which are critical in smaller-scale analyses or scenarios where discontinuities dominate the rock mass behaviour, making them essential in such cases (Jing and Hudson, 2002).

In discontinuum modelling, the rock mass is represented as a collection of discrete blocks, which are separated by discontinuities such as joints or bedding

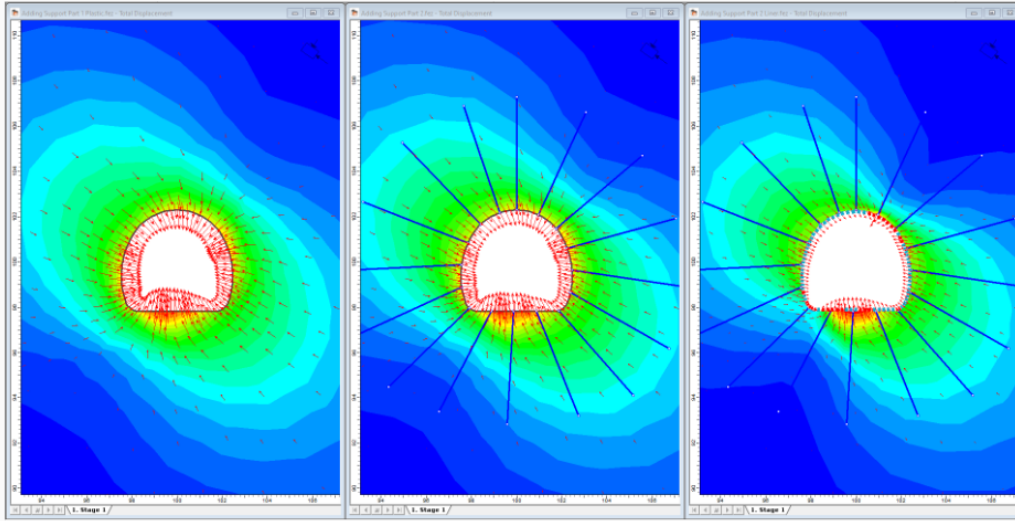


Figure 3.3.1: A horseshoe-shaped drift with an approximate span of 5 meters. The level of support increases from left to right, starting with no support, followed by bolting, and finally bolting combined with shotcrete (*RS2 Tutorials / Adding Support 2024*).

planes. These blocks are treated as deformable bodies, with the interfaces between them modeled as potential zones of slip, separation, or rotation. Individual blocks are free to translate or rotate independently, and new contact points can form as blocks move relative to one another. This ability to simulate block interactions and large-scale displacements makes discontinuum methods highly effective for analyzing mechanisms such as block detachment, sliding, or rotation (Jing and Hudson, 2002).

Some popular discontinuum methods are Discrete Element Method (DEM) and Discrete Fracture Network Method (DFN) (Jing and Hudson, 2002). The next subsection briefly introduces DEM.

Discrete Element Method

The Discrete Element Method (DEM) started to develop in the field of rock mechanics applications due to its requirement for modelling discontinuous behaviour. Unlike continuum approaches, DEM treats the material as a collection of particles or blocks rather than a continuous medium. These particles interact dynamically as deformation occurs, allowing the method to

simulate both the discontinuities and the rock blocks simultaneously (Nikolić et al., 2016).

DEM explicitly models the rock mass as discrete blocks that interact through joints or fractures, enabling the method to capture complex behaviours such as de-bonding and detachment at interfaces. The equations of motion are solved for each block, and the model calculates forces based on properties like friction, cohesion, and normal stiffness. This makes DEM particularly effective in scenarios where failure is dominated by fractures or blocky structures (Nikolić et al., 2016).

Several DEM-based approaches exist, differing primarily in the shapes of the elements, methods for calculating contact forces, and techniques for recognizing contacts. The displacement field in DEM is not physically continuous. Instead, individual blocks can translate or rotate independently, with slip or separation occurring at their interfaces. This ability to simulate block movement and interaction makes DEM invaluable for modelling rock masses with significant jointing or blocky structures, where traditional methods like FEM may fail to capture the critical behaviours (Nikolić et al., 2016).

3.3.3 Applications and Limitations

Numerical modelling complements traditional classification and characterization systems such as RMR, Q, and GSI and analytical methods such as CCM by providing a more detailed understanding of rock mass behaviour.

One of the key advantages of numerical modelling is its ability to simulate both 2D and 3D conditions, depending on the geometric characteristics of the problem. 2D models are effective for uniform systems, such as long tunnels with consistent cross-sections, while 3D models are essential for analyzing irregular geometries or variations along multiple dimensions. Numerical methods also allow engineers to observe how the support interacts dynamically with the rock mass, enabling better assessment of stability and design performance (Nikolić et al., 2016).

However, numerical modelling is highly dependent on the quality of the input data. It is clear that poor or incomplete data can lead to inaccurate results, highlighting the importance of site-specific characterization and reliable input parameters. Back-analysis, where observed deformation is compared with model predictions, can help refine the model and improve its reliability, even

when the initial data is imperfect (Jing and Hudson, 2002).

It is important to note that numerical models provide a tendency or a general behaviour of the system rather than exact numerical values, and their computed results should be viewed as approximations rather than absolute truths. However, in most engineering applications, the accuracy of these solutions satisfies the practical requirements (Jing and Hudson, 2002).

The choice of modelling method, whether continuum, discontinuum or hybrid, depends on the specific problem. Continuum methods are suitable for rock masses with non or a few discontinuities, while discontinuum methods are better suited for fractured or blocky systems. Very fractured rock can be assumed to behave pseudo-continuous so that continuum methods can be used (C. Li, 2021).

To demonstrate the selection of an appropriate method, Figure 3.3.2 presents four distinct scenarios associated with underground excavations.

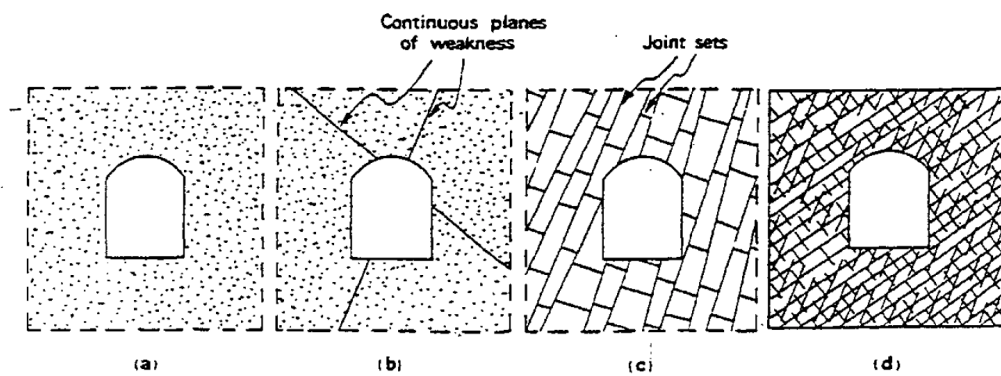


Figure 3.3.2: The figure highlights different rock mass conditions, which significantly influence the choice of numerical methods (C. Li, 2021).

For the first scenario, (a), continuum methods can be applied because the displacements are predicted to be continuous, with no discontinuities in the rock mass (C. Li, 2021).

In the second scenario, (b), the material contains a few discontinuities with large spacing relative to the dimensions of the excavation. Continuum methods can still be applied in this case because the large intact blocks behave as a continuum, even though slip or separation may occur along the planes of weakness (C. Li, 2021).

In these two scenarios, BEM and FEM would be the most applicable techniques for analyzing elastic and elasto-plastic deformations, respectively (C. Li, 2021). Additionally, for case (b), the advanced FEM approaches discussed earlier in 3.3.1 could be particularly beneficial (Nikolić et al., 2016).

In the third scenario, (c), the rock mass contains joint sets with smaller spacing compared to (b), and the spacing is much smaller than the size of the excavation. This makes discontinuous methods necessary, as slip and separation along the joints, as well as rotation of individual blocks, will determine the displacements. For this case, DEM is the most appropriate approach (C. Li, 2021).

For the fourth scenario, (d), the rock mass is highly fractured, and the displacement field can be treated as pseudo-continuous. In this situation, a system that is inherently discrete or discontinuous is modeled as if it were continuous to simplify the analysis. A ubiquitous joint, elastoplastic model using FEM would be suitable for this case (C. Li, 2021).

Chapter 4

Conclusions

While empirical and analytical methods are often useful for initial assessments, they assume idealised conditions and cannot fully capture the complexities of rock masses, such as irregular geometries, varying material properties and stresses, or the presence of fractures and joints. Numerical modelling, by contrast, excels in addressing these complexities, making it an indispensable tool in modern rock engineering.

Based on the findings and opinions of numerous authors, it is evident that a deterministic value can be highly useful in the analysis of rock stability problems. However, considering the inherent variability of rock mass behaviour, it is more realistic to perform a probabilistic analysis using a range of values rather than a single value. This approach provides better insight into the uncertainties involved while also offering an understanding of the sensitivity of the system. This applies to all the methods introduced in this report.

It is also clear that none of these methods will provide an optimized design on their own. Only through a combination of methods, careful comparison, and sound engineering judgment can one achieve a robust and reliable design that accounts for the complexities and uncertainties of rock mass behaviour.

References

- Abbas, Syed Muntazir and Heinz Konietzky (Jan. 15, 2015). “Rock Mass Classification Systems”. In: p. 43.
- Amadei, Bernard and Ove Stephansson (1997). *Rock Stress and Its Measurement*. Dordrecht: Springer Netherlands. ISBN: 978-94-010-6247-3 978-94-011-5346-1. DOI: 10.1007/978-94-011-5346-1. URL: <http://link.springer.com/10.1007/978-94-011-5346-1> (visited on 11/08/2024).
- Barton, N., R. Lien, and J. Lunde (Dec. 1, 1974). “Engineering classification of rock masses for the design of tunnel support”. In: *Rock mechanics* 6.4, pp. 189–236. ISSN: 1434-453X. DOI: 10.1007/BF01239496. URL: <https://doi.org/10.1007/BF01239496> (visited on 10/30/2024).
- Bieniawski, Z. T. (1974). “GEOMECHANICS CLASSIFICATION OF ROCK MASSES AND ITS APPLICATION IN TUNNELING.” In: pp. 27–32.
- (Aug. 24, 1989). *Engineering Rock Mass Classifications: A Complete Manual for Engineers and Geologists in Mining, Civil, and Petroleum Engineering*. Google-Books-ID: pejDUvjjwPdMC. John Wiley & Sons. 274 pp. ISBN: 978-0-471-60172-2.
- (Jan. 1, 1993). “22 - Classification of Rock Masses for Engineering: The RMR System and Future Trends”. In: *Rock Testing and Site Characterization*. Ed. by JOHN A. Hudson. Oxford: Pergamon, pp. 553–573. ISBN: 978-0-08-042066-0. DOI: 10.1016/B978-0-08-042066-0.50028-8. URL: <https://www.sciencedirect.com/science/article/pii/B9780080420660500288> (visited on 10/22/2024).
- C. Li, Charlie (2021). *TGB 4210 Rock Mechanics (Basic course)*.
- Carranza-Torres, C. and C. Fairhurst (Apr. 1, 2000). “Application of the Convergence-Confinement method of tunnel design to rock masses that satisfy the Hoek-Brown failure criterion”. In: *Tunnelling and Underground Space Technology* 15.2, pp. 187–213. ISSN: 0886-7798. DOI: 10.1016/S0886-7798(00)00046-8. URL: <https://www.sciencedirect.com/science/article/pii/S0886779800000468> (visited on 11/13/2024).

- Celada, B et al. (2014). "Innovating tunnel design by an improved experience-based RMR system". In: *Proceedings of the world tunnel congress*, pp. 1–9. URL: http://www.cdiam.es/doc/Articulos/BIENIAWSKI-CELADA_INNOVATING_RMR14.pdf (visited on 10/23/2024).
- Fama, MARY E. DUNCAN (Jan. 1, 1993). "3 - Numerical Modeling of Yield Zones in Weak Rock". In: *Analysis and Design Methods*. Ed. by CHARLES Fairhurst. Oxford: Pergamon, pp. 49–75. ISBN: 978-0-08-040615-2. DOI: 10.1016/B978-0-08-040615-2.50009-5. URL: <https://www.sciencedirect.com/science/article/pii/B9780080406152500095> (visited on 12/12/2024).
- Hoek, E and Paul Marinos (May 1, 2007). "A brief history of the development of the Hoek-Brown failure criterion". In: *Soils and Rocks* 30.2, pp. 85–95. ISSN: 19809743, 26755475. DOI: 10.28927/SR.302085. URL: <https://soilsandrocks.com/sr-302085> (visited on 10/30/2024).
- Hoek, E. and E. T. Brown (June 1, 2019). "The Hoek–Brown failure criterion and GSI – 2018 edition". In: *Journal of Rock Mechanics and Geotechnical Engineering* 11.3, pp. 445–463. ISSN: 1674-7755. DOI: 10.1016/j.jrmge.2018.08.001. URL: <https://www.sciencedirect.com/science/article/pii/S1674775518303846> (visited on 10/15/2024).
- Hoek, E., P. K. Kaiser, and W. F. Bawden (Jan. 1, 2000). *Support of Underground Excavations in Hard Rock*. Google-Books-ID: RefFNXdxt7wC. CRC Press. 240 pp. ISBN: 978-90-5410-186-4.
- Hoek, Evert (2007). *Practical Rock Engineering*. RocScience.
- Hoek, Evert, T.G. Carter, and M.S. Diederichs (2024). *Quantification of the Geological Strength Index Chart*. URL: https://www.researchgate.net/publication/288349401_Quantification_of_the_Geological_Strength_Index_Chart (visited on 12/13/2024).
- Hoek, Evert and P. Kaiser (Jan. 1, 1995). "Support of Underground Excavation in Hard Rock". In.
- Jing, L. and J. A. Hudson (June 1, 2002). "Numerical methods in rock mechanics". In: *International Journal of Rock Mechanics and Mining Sciences*. Numerical Methods in Rock Mechanics 39.4, pp. 409–427. ISSN: 1365-1609. DOI: 10.1016/S1365-1609(02)00065-5. URL: <https://www.sciencedirect.com/science/article/pii/S1365160902000655> (visited on 12/09/2024).
- Kargar, Ali Reza (Dec. 1, 2019). "An analytical solution for circular tunnels excavated in rock masses exhibiting viscous elastic-plastic behavior". In: *International Journal of Rock Mechanics and Mining Sciences* 124, p. 104128. ISSN: 1365-1609. DOI: 10.1016/j.ijrmms.2019.104128. URL: <https://www.sciencedirect.com/science/article/pii/S1365160919301984> (visited on 11/13/2024).

- Karpuz, Celal and Hakan Basarir (Nov. 2015). "Strata Control for Underground Coal Mines". In: *Coal Production and Processing Technology*. CRC Press, pp. 161–184.
- Labuz, Joseph F. and Arno Zang (2015). "Mohr–Coulomb Failure Criterion". In: *The ISRM Suggested Methods for Rock Characterization, Testing and Monitoring: 2007-2014*. Ed. by R. Ulusay. Cham: Springer International Publishing, pp. 227–231. ISBN: 978-3-319-07713-0. DOI: 10.1007/978-3-319-07713-0_19. URL: https://doi.org/10.1007/978-3-319-07713-0_19 (visited on 11/04/2024).
- Lorig, L. J. et al. (May 13, 2013). *Guidelines for numerical modelling of rock support for mines*. Conference Name: Ground Support 2013: Seventh International Symposium on Ground Support in Mining and Underground Construction, 2013 13-15 May, Perth. Australian Centre for Geomechanics, pp. 81–105. DOI: 10.36487/ACG_rep/1304_04_Lorig. URL: https://papers.acg.uwa.edu.au/p/1304_04_Lorig/ (visited on 12/11/2024).
- Marinos, Paul and Evert Hoek (n.d.). "GSI: A GEOLOGICALLY FRIENDLY TOOL FOR ROCK MASS STRENGTH ESTIMATION". In: () .
- Marinos, V., P. Marinos, and E. Hoek (Apr. 1, 2005). "The geological strength index: applications and limitations". In: *Bulletin of Engineering Geology and the Environment* 64.1, pp. 55–65. ISSN: 1435-9537. DOI: 10.1007/s10064-004-0270-5. URL: <https://doi.org/10.1007/s10064-004-0270-5> (visited on 12/12/2024).
- Milne, D., J. Hadjigeorgiou, and R. Pakalnis (Oct. 1, 1998). "Rock mass characterization for underground hard rock mines". In: *Tunnelling and Underground Space Technology* 13.4, pp. 383–391. ISSN: 0886-7798. DOI: 10.1016/S0886-7798(98)00081-9. URL: <https://www.sciencedirect.com/science/article/pii/S0886779898000819> (visited on 12/14/2024).
- Nikolić, Mijo, Tanja Roje-Bonacci, and Adnan Ibrahimbegović (Apr. 27, 2016). "Overview of the numerical methods for the modelling of rock mechanics problems". In: *Tehnički vjesnik* 23.2. Publisher: Sveučilište u Slavonskom Brodu, Stojarski fakultet, pp. 627–637. ISSN: 1330-3651, 1848-6339. DOI: 10.17559/TV-20140521084228. URL: <https://hrcak.srce.hr/clanak/231206> (visited on 12/09/2024).
- Palmström, Arild (Mar. 2008). *COMPARING THE RMR, Q, AND RMi CLASSIFICATION SYSTEMS*. URL: https://rockmass.net/files/correlation_Q-RMR-RMi-1.pdf.
- (n.d.). *Short on the RMR (Rock Mass Rating) system*. URL: https://www.rockmass.net/files/short_on_RMR-system.pdf.
- Paraskevopoulou, Chrysothemis and Mark Diederichs (Jan. 1, 2018). "Analysis of time-dependent deformation in tunnels using the Convergence-Confinement Method". In: *Tunnelling and Underground Space Technology*

- 71, pp. 62–80. ISSN: 0886-7798. DOI: 10.1016/j.tust.2017.07.001. URL: <https://www.sciencedirect.com/science/article/pii/S0886779816307878> (visited on 11/13/2024).
- Pells, P. J. et al. (Jan. 16, 2017). “Rock quality designation (RQD): time to rest in peace”. In: *Canadian Geotechnical Journal*. Publisher: NRC Research Press. DOI: 10.1139/cgj-2016-0012. URL: <https://cdnsciencepub.com/doi/10.1139/cgj-2016-0012> (visited on 10/08/2024).
- Rehman, Hafeezur et al. (Aug. 2018). “Review of Rock-Mass Rating and Tunneling Quality Index Systems for Tunnel Design: Development, Refinement, Application and Limitation”. In: *Applied Sciences* 8.8. Number: 8 Publisher: Multidisciplinary Digital Publishing Institute, p. 1250. ISSN: 2076-3417. DOI: 10.3390/app8081250. URL: <https://www.mdpi.com/2076-3417/8/8/1250> (visited on 10/24/2024).
- Ritter, Wilhelm (1879). *Die Statik der Tunnelgewölbe*. Berlin: Springer.
- RockMass (2024). URL: <https://rockmass.net/rock-properties/> (visited on 11/18/2024).
- RS2 / 2D Geotechnical Finite Element Analysis / Rocscience (2024). URL: <https://www.rocscience.com/software/rs2> (visited on 12/11/2024).
- RS2 Tutorials / Adding Support (2024). URL: <https://www.rocscience.com/help/rs2/tutorials/support/adding-support> (visited on 12/11/2024).
- RS3 / 3D Finite Element Software For Advanced Analysis / Rocscience (2024). URL: <https://www.rocscience.com/software/rs3> (visited on 12/11/2024).
- Singh, B. and R. K. Goel (May 5, 1999). *Rock Mass Classification: A Practical Approach in Civil Engineering*. Google-Books-ID: SOfs7wDYxTcC. Elsevier. 282 pp. ISBN: 978-0-08-054065-8.
- Using the Q-system (2022). *Using the Q-system - Rock mass classification and support design*. URL: https://www.ngi.no/globalassets/bilder/forskning-og-radgivning/bygg-og-anlegg/handbook-the-q-system-may-2015-nettutg_update-june-2022.pdf (visited on 10/29/2024).
- Vásárhelyi, Balázs and Dorottya Kovács (2017). “Empirical methods of calculating the mechanical parameters of the rock mass”. In: *Periodica Polytechnica Civil Engineering* 61.1. Number: 1, pp. 39–50. ISSN: 1587-3773. DOI: 10.3311/PPci.10095. URL: <https://www.pp.bme.hu/ci/article/view/10095> (visited on 12/13/2024).
- Zhang, Lianyang (Mar. 1, 2017). “Evaluation of rock mass deformability using empirical methods – A review”. In: *Underground Space* 2.1, pp. 1–15. ISSN: 2467-9674. DOI: 10.1016/j.undsp.2017.03.003. URL: <https://www.sciencedirect.com/science/article/pii/S2467967416300253> (visited on 12/13/2024).

- Zhang, Qi et al. (Jan. 1, 2019). “Quantitative assessments of the correlations between rock mass rating (RMR) and geological strength index (GSI)”. In: *Tunnelling and Underground Space Technology* 83, pp. 73–81. ISSN: 0886-7798. DOI: 10.1016/j.tust.2018.09.015. URL: <https://www.sciencedirect.com/science/article/pii/S0886779818304395> (visited on 12/14/2024).

Appendices

Appendix A

RQD

Rock mass designation, RQD, is a well known index for classifying rock mass quality, originally calculated from diamond drill core samples. It was introduced by Don Deer in 1964, and was later incorporated in well known rock mass classification systems like RMR, Q, and GSI, making it an important parameter in rock mechanics design all over the world. RQD is calculated on cores with a 50mm diameter as:

$$RQD = \frac{\sum L_i}{L} \cdot 100$$

where L_i is the length each individual intact core piece that is 100 mm or longer, and L is the total length of the core run.

RQD Rock Mass Classification	Range
Excellent	$\geq 90\% - 100\%$
Good	$\geq 75\% - 90\%$
Fair	$\geq 50\% - 75\%$
Poor	$\geq 25\% - 50\%$
Worse	$\leq 25\%$

Table A.0.1: RQD Rock Mass Classification

The index was developed by Deere and his colleagues in 1964 and 1965 while studying granite formations at the Nevada Test Site for nuclear bomb experiments. Its purpose was to distinguish between high-quality and poor-quality

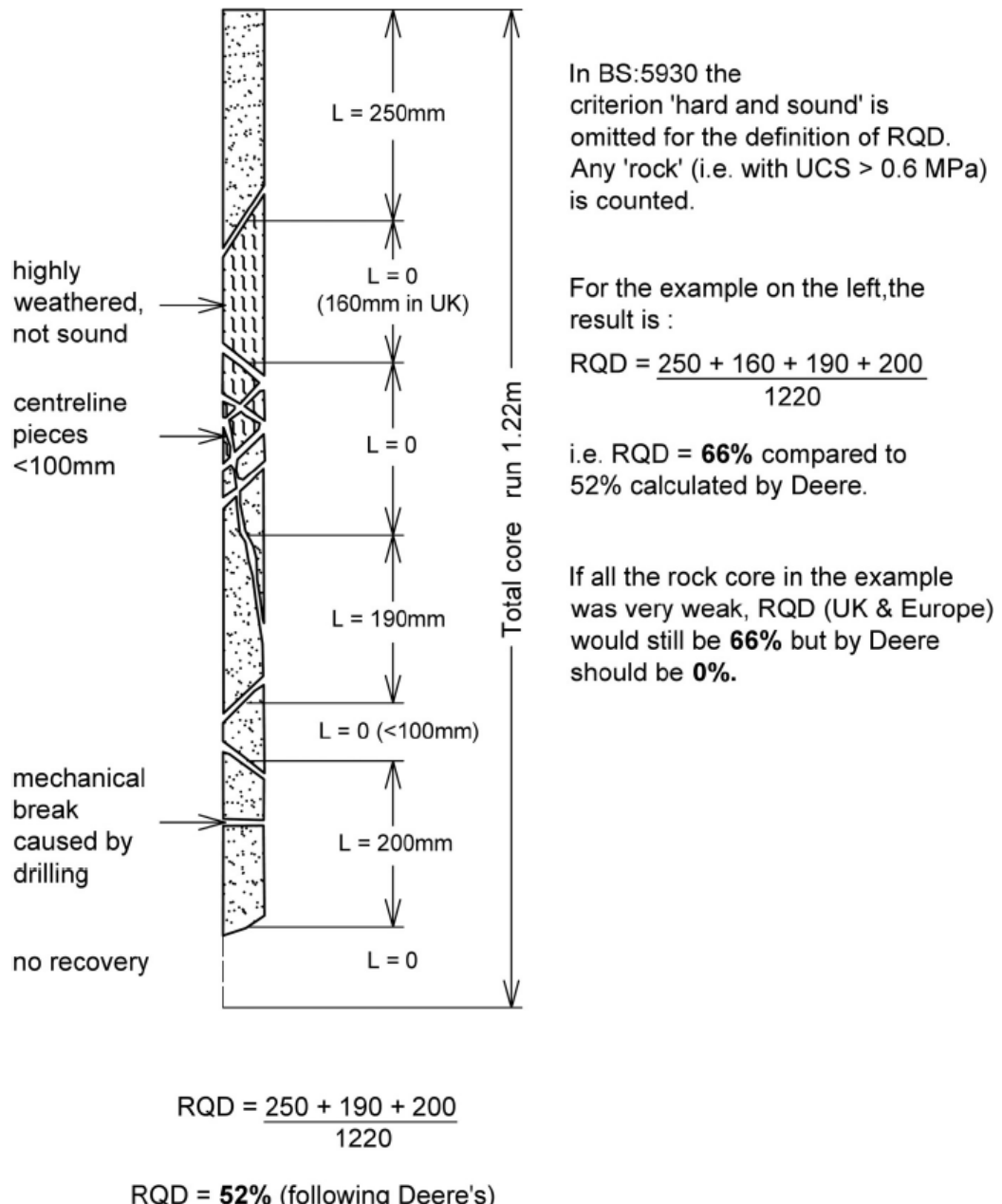


Figure A.0.1: RQD Example

rock during core logging, providing a more accurate assessment than relying solely on core recovery.

In a review of RQD, after 20 years of its development, Deer highlighted three key aspects of RQD:

1. RQD measures rock mass quality from a 55 mm double-tube core over the length of the core run.
2. Only core pieces longer than 100 mm, separated by natural fractures, should be included. Fractures caused by drilling are ignored.
3. Core pieces that are not "hard and sound" should not be included in the RQD, even if they are longer than 100 mm.

RQD was intended to measure more than fracture spacing; it shows the percentage of intact, good-quality rock, excluding weathered or fractured parts.

Deere defined "hard and sound" as rock that is not highly weathered or weakened. Highly weathered rock, which can be crumbled by hand, should never be included in the RQD calculation. Moderately weathered rock may be included but should be marked with an asterisk (RQD*), although this practice is not always followed in the field.

When using the RQD index to define rock mass quality, there are uncertainties, sources of confusion, and potential errors pointed out by Deer, that one should be aware of:

- Measurements are often taken after core boxing, which can cause small fractures and result in a lower RQD. Core discing, where the rock core breaks into thin, disk-like pieces due to stress release after drilling, is one example of this.
- Standard practice is to measure RQD by core run, though logging by rock type is recommended.
- Directional bias can cause under-sampling of defects when joints run parallel to the borehole.
- There's confusion over the definition of "natural mechanical fractures" in certain rocks like schists and shales.

- Well-defined discontinuities with tensile strength should be ignored in RQD calculations, but this can cause confusion.

Pells et al., 2017 recognize these points, but emphasize that the most important reason for errors in RQD values is the frequent disregard for the "hard and sound" rock criterion. In the UK and Europe, this criterion is often ignored, leading to higher RQD values, with potentially dangerous consequences for support design in weak rock masses. Additionally, estimating RQD from photographs is challenging and deviates from the original method.

When RQD needs to be calculated but core samples are not available, some choose to estimate RQD from rock exposures. This does not align with Deere's original method, which was based on core samples. It is challenging to assess Deere's "hard and sound" criterion in the field, as well as whether a discontinuity has zero tensile strength, which would cause a break. Another issue is that certain fractures may not be detected when observed from a specific direction. To demonstrate the difficulties, Pells et al., 2017 present a study where 13 professionals estimated the RQD value of three exposures. The results showed significant variation in RQD values, highlighting the challenges of estimating RQD from rock exposures. The result can be seen in Figure A.0.2.

Pells et al., 2017 recommends that RQD should be phased out in rock mass classification. RQD definitions have become inconsistent worldwide, and in many places no longer follow Don Deere's original method. In most cases, RQD must be estimated from rock exposures, which often leads to errors and subjective differences. The limitations of RQD have already been recognized by the creators of RMR, who have suggested replacing it with fracture frequency. It has also been demonstrated that GSI can be estimated from Hoek's charts just as accurately as through calculations involving RQD and other components.

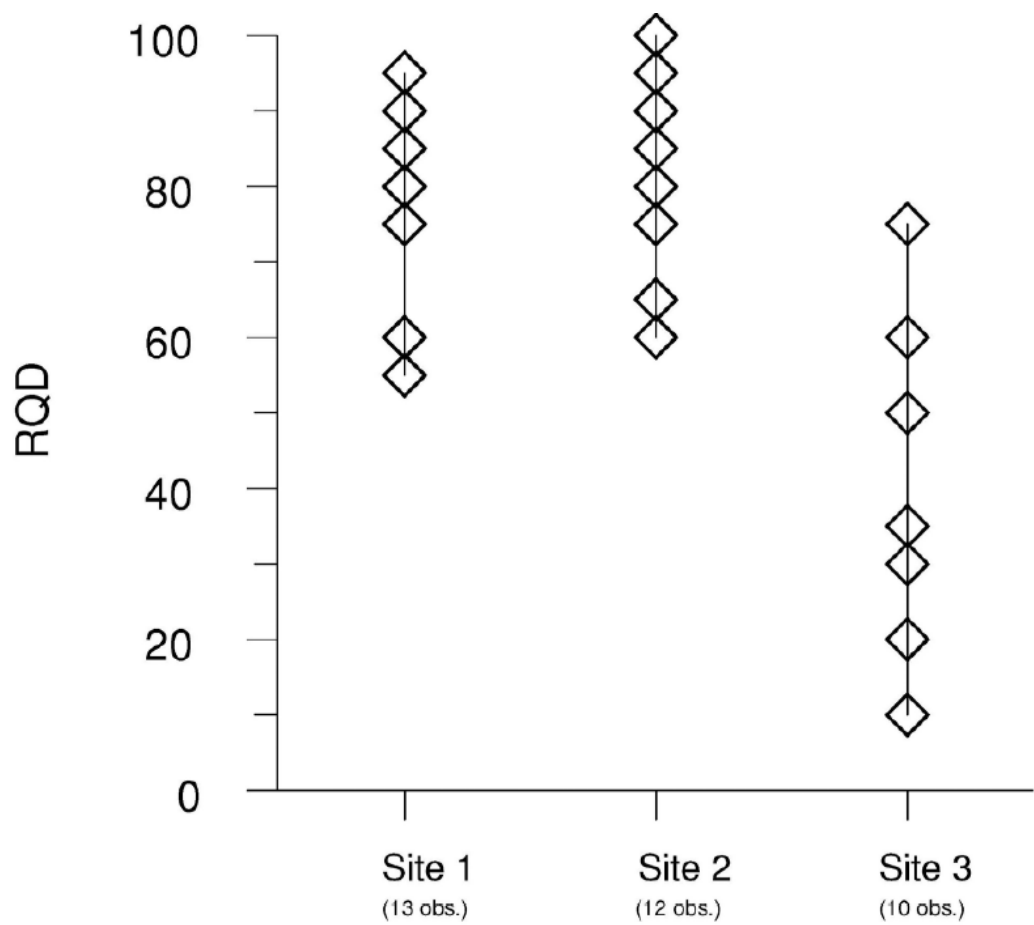


Figure A.0.2: RQD Sydney test

Appendix B

RMR₈₉ and RMR₁₄ Tables

The latest update, RMR14, introduced in 2014, includes revised parameters, an updated rating system, and an improved structure (Celada et al., 2014). This new system retains the parameters *Uniaxial Compressive Strength of Intact Rock* and *Water Effect* from RMR89 and combines RQD with Discontinuity Spacing to define the parameter *Number of Discontinuities per Meter* (Celada et al., 2014).

The new parameters of RMR14 is revised *Discontinuities condition* and the *Rock alterability* due to water (swelling). The discontinuities condition is rated based on four aspects: Continuity, Roughness, Gouge infilling and Weathering. The rock alterability is found using a Slake Durability Test (Celada et al., 2014). These five parameters make up the new RMR_b.

RMR14 can be calculated using Equation B.1.

$$\text{RMR}_{14} = (\text{RMR}_b + F_0) \cdot F_s \cdot F_e \quad (\text{B.1})$$

- RMR_b = RMR basic of the rock mass, without an effect of excavation.
- F_0 = Adjustment factor like R_6 in RMR89, accounting for tunnel orientation relative to rock discontinuities. Value is found in a given table and is always negative.
- F_e = Adjustment factor based on the excavation method's impact on rock stability.

- F_e = Adjustment factor reflecting stress-strain behavior at the tunnel face during excavation.

When using the drill and blast excavation method, F_e is assigned a value of 1. The appropriate equation for calculating F_e depends on the RMR₈₉ value. For mechanical excavation methods, which have a positive influence on tunneling performance, F_e can be determined using Equations B.2 and B.3:

$$F_e = 1 + 2 \cdot \left(\frac{RMR_{89}}{100} \right)^2, \quad RMR_{89} < 40 \quad (\text{B.2})$$

$$F_e = 1.32 - \frac{\sqrt{RMR_{89} - 40}}{25}, \quad RMR_{89} > 40 \quad (\text{B.3})$$

Because of operational errors, in addition to the effects of yielding of the rock mass, the estimated RMR at the excavated face is often significantly lower than the value determined in the design phase. Therefore the F_s parameter is introduced to account for these errors. To determine the F_s value, it is necessary to calculate the ICE (Índice de Comportamiento Elástico), which describes the elastic response of the rock:

$$ICE = \frac{3704 \cdot \sigma_c \cdot e^{\frac{RMR-100}{24}}}{(3 - K_0) \cdot H} \cdot F, \quad K_0 \leq 1 \quad (\text{B.4})$$

$$ICE = \frac{3704 \cdot \sigma_c \cdot e^{\frac{RMR-100}{24}}}{(3 \cdot K_0 - 1) \cdot H} \cdot F, \quad K_0 \geq 1 \quad (\text{B.5})$$

where

- σ_c = intact rock uniaxial compressive strength (UCS) (MPa),
- K_0 = ratio of the horizontal to vertical virgin stress.,
- H = tunnel depth (m),
- F = shape coefficient found in table.

Having obtained an ICE value, one can easily calculate the corresponding F_s value by using the following equations:

$$F_s = 1.3, \quad ICE < 15 \quad (\text{B.6})$$

$$F_s = \frac{2.3\sqrt{100 - ICE}}{7.1 + \sqrt{100 - ICE}}, \quad 15 < ICE < 70 \quad (\text{B.7})$$

$$F_s = 1, \quad ICE > 70 \quad (\text{B.8})$$

Celada et al., 2014 provides a chart illustrating the strong correlation between RMR89 and RMR14. This relationship is defined by Equation B.9 and demonstrates a high correlation coefficient of $R^2 = 0.982$.

$$\text{RMR}_{14} = 1.1 \cdot \text{RMR}_{89} + 2 \quad (\text{B.9})$$

INPUT PARAMETERS TO RMR₁₉₈₉
(from Bieniawski, 1989)

PARAMETER		Range of values // RATINGS					
1 rock material	Strength of intact rock material	> 10 MPa Uniaxial com- pressive strength	> 10 MPa > 250 MPa	4 - 10 MPa 100 - 250 MPa	2 - 4 MPa 50 - 100 MPa	1 - 2 MPa 25 - 50 MPa	For this low range uniaxial compr. strength is preferred
	RATING	15	12	7	4	2	1 - 5 MPa < 1 MPa
	Drill core quality RQD	90 - 100%	75 - 90%	50 - 75%	25 - 50%	< 25%	
2	RATING	20	17	13	8	5	
	Spacing of discontinuities	> 2 m	0.6 - 2 m	200 - 600 mm	60 - 200 mm	< 60 mm	
3 Condition of discontinuities	RATING	20	15	10	8	5	
	Length, persistence	< 1 m	1 - 3 m	3 - 10 m	10 - 20 m	> 20 m	
	Rating	6	4	2	1	0	
	Separation	none	< 0.1 mm	0.1 - 1 mm	1 - 5 mm	> 5 mm	
	Rating	6	5	4	1	0	
	Roughness	very rough	rough	slightly rough	smooth	slickensided	
	Rating	6	5	3	1	0	
	Infilling (gouge)	none	Hard filling		Soft filling		
	Rating	6	4	2	2	> 5 mm	
4 Ground water	Weathering	unweathered	slightly w.	moderately w.	highly w.	decomposed	
	Rating	6	5	3	1	0	
	Inflow per 10 m tunnel length	none	< 10 litres/min	10 - 25 litres/min	25 - 125 litres/min	> 125 litres /min	
	p_w / σ_1	0	0 - 0.1	0.1 - 0.2	0.2 - 0.5	> 0.5	
5	General conditions	completely dry	damp	wet	dripping	flowing	
	RATING	15	10	7	4	0	
	p_w = joint water pressure; σ_1 = major principal stress						

RATING ADJUSTMENT FOR DISCONTINUITY ORIENTATIONS

		Very favourable	Favourable	Fair	Unfavourable	Very unfavourable
RATINGS	Tunnels	0	-2	-5	-10	-12
	Foundations	0	-2	-7	-15	-25
	Slopes	0	-5	-25	-50	-60

ROCK MASS CLASSES DETERMINED FROM TOTAL RATINGS

Rating	100 - 81	80 - 61	60 - 41	40 - 21	< 20
Class No.	I	II	III	IV	V
Description	VERY GOOD	GOOD	FAIR	POOR	VERY POOR

MEANING OF ROCK MASS CLASSES

Class No.	I	II	III	IV	V
Average stand-up time	10 years for 15 m span	6 months for 8 m span	1 week for 5 m span	10 hours for 2.5 m span	30 minutes for 1 m span
Cohesion of the rock mass	> 400 kPa	300 - 400 kPa	200 - 300 kPa	100 - 200 kPa	< 100 kPa
Friction angle of the rock mass	< 45°	35 - 45°	25 - 35°	15 - 25°	< 15°

2011-03-04

Figure B.0.1: RMR₈₉ input parameters (Bieniawski, 1989).

RMR classification guide for excavation and support in rock tunnels.
 Tunnel shape: horseshoe; width: 10m. Vertical stress: below 25MPa.
 (from Bieniawski, 1989)

Rock mass class	Excavation by drill & blast	Rock support (for 10m wide tunnels)		
		Rock bolts (20mm diam., fully bonded)	Shotcrete	Steel sets
1.Very good rock RMR: 81 - 100	Full face: 3m advance		Generally no support required except for occasional spot bolting	
2.Good rock RMR: 61 - 80	Full face: 1.0 - 1.5m advance; Complete support 20m from face	Locally bolts in crown, 3m long, spaced 2.5m with occasional wire mesh	50mm in crown where required	None
3.Fair rock RMR: 41- 60	Top heading and bench: 1.5 - 3m advance in top heading; Commence support after each blast; Commence support 10m from face	Systematic bolts 4m long, spaced 1.5 - 2m in crown and walls with wire mesh in crown	50 - 100mm in crown, and 30mm in sides	None
4.Poor rock RMR: 21- 40	Top heading and bench: 1.0 - 1.5m advance in top heading; Install support concurrently with excavation - 10m from face	Systematic bolts 4 - 5m long, spaced 1-1.5m in crown and walls with wire mesh	100-150mm in crown and 100mm in sides	Light ribs spaced 1.5m where required
5.Very poor rock RMR < 21	Multiple drifts: 0.5 - 1.5m advance in top heading; Install support concurrently with excavation; shotcrete as soon as possible after blasting	Systematic bolts 5 - 6m long, spaced 1 - 1.5m in crown and walls with wire mesh. Bolt the invert	150 - 200mm in crown, 150mm in sides, and 50mm on face	Medium to heavy ribs spaced 0.75m with steel lagging and forepoling if required. Close invert

2011-03-04

Figure B.0.2: Support recommendations by RMR₈₉ (Bieniawski, 1989).